Coordination Chemistry Reviews 254 (2010) 2342–2362

Contents lists available at ScienceDirect

Coordination Chemistry Reviews

journal homepage: www.elsevier.com/locate/ccr

Review

Supramolecular architectures of porphyrins on surfaces: The structural evolution from 1D to 2D to 3D to devices

Stefan Mohnani[a,b], Davide Bonifazi[a,b,*]

[a] INSTM UdR di Trieste and Dipartimento di Scienze Farmaceutiche, Università degli Studi di Trieste, 34127 Trieste, Italy
[b] Department of Chemistry, University of Namur (FUNDP), B-5000 Namur, Belgium

Contents

ARTICLE INFO

Article history:
Received 1 February 2010
Accepted 15 May 2010
Available online 24 May 2010

Dedicated to Professor Alain Krief.

Keywords:
Porphyrin
STM
Liquid-solid
UHV-solid
Interface
Surface
Self-assembly
Supramolecular chemistry
Nano-patterned surfaces

ABSTRACT

Tetrapyrrolic macrocycles, such as porphyrins, belong to a class of distinctively multifunctional biomolecules playing a central role in fundamental natural processes such as electron transfer, oxygen transfer, and light-harvesting, and their use to mimic these biological events in nanotechnological devices would be of obvious benefit. Despite the synthetic and physical achievements, a technical impediment towards the exploitation of such porphyrin-based architectures in applicative devices is that they cannot be singularly addressed in solution or at solid state, as they must be interfaced with the external world. They also need to show durability and functionality under the extreme conditions that are normally used in operating practical devices. Typically, porphyrin architectures have been investigated in solution, however, the tendency in current research is to deposit functional porphyrin derivatives on the surfaces of bulk materials such as metals or semiconductors and investigate the resultant hybrid surfaces using STM. In this review, we have illustrated the trends in supramolecular nanopatterning of porphyrin derivatives at different interfaces. Various strategies for the construction of nanoscale architectures at different interfaces are described along the course of the review, including sublimation under UHV conditions, adlayer formation by immersion of a surface in a liquid or deposition of a solution. The discussion of assemblies on surfaces commences with a description of the very recent developments in the remarkably precisely controlled construction of discrete assemblies on surfaces under UHV conditions. Subsequently, extended 2D arrays formed in both ambient conditions at the liquid–solid interface, as well as under UHV conditions have been discussed along with the ability of certain 2D self-assemblies to accommodate guest molecules. The last section of the review deals with porphyrin assemblies featuring three-dimensional properties, with a particular focus on those systems in which the third-dimension introduces functionality such as gas-storage, catalysis and a molecular motor.

1. Introduction

Electronic devices based on inorganic semiconductors have been part of our daily lives for the last 60 years [1]. However, now, in the beginning of the new millennium the increased development and knowledge of organic semiconductors has led to a tendency to explore alternative avenues than inorganic semiconductor and focus on the creation of electronic devices based on

* Corresponding author at: Department of Chemistry, University of Namur (FUNDP), B-5000 Namur, Belgium.
E-mail address: davide.bonifazi@fundp.ac.be (D. Bonifazi).

0010-8545/$ – see front matter © 2010 Elsevier B.V. All rights reserved.
doi:10.1016/j.ccr.2010.05.006

organic molecules. In order to construct such hybrid molecular-based nanoscale devices, methods for the controlled fabrication of well-defined organic nanostructures need to be developed [2–4]. One of the most promising methods to date is the "bottom-up" approach, wherein ordered structures with nanometer precision over an extended large scale can be constructed. The concept of this approach is to exploit multiple non-covalent interactions between pre-engineered molecules, which through their selective recognition are able to form convergent assemblies. Due to the intermolecular interactions, a dynamic equilibrium exists between the individual molecular components and the assembly as a whole thus leading to thermodynamically controlled multistable systems the reversibility of which allows for the self-rearrangement and self-correction of the components within the assembled structure. This so-called 'self-healing' contributes to the formation of long-range ordered and defect-free systems barely accessible through conventional covalent synthesis [5–13]. In this respect, promising classes of molecules for the formation of functional supramolecular architectures are porphyrins and their derivatives. Porphyrins are related to the natural di- and tetra-hydrotetrapyrrolic macrocycles e.g. chlorins, bacteriochlorins, porphyrinogens, and protoporphyrins. These distinctively multifunctional biomolecules are generally present as metallocomplexes where the four nitrogen atoms are coordinated to a metal atom such as Fe(III) or Mg(II). It is the combination of a rigid planar aromatic organic ligand and the redox properties of the metal which allows the natural tetrapyrrolic macrocycles to play a central role in electron transfer, oxygen transfer, and light-harvesting processes in metalloproteins [14–18]. Indeed, utilising such molecules to mimic biological events in nanotechnological devices would be of obvious benefit, however, due to the presence of two or more saturated carbon atoms in the macrocyclic scaffold, chlorins are not easily reproduced synthetically. Instead, fully conjugated tetrapyrrolic macrocycles such as porphyrins, have been by far the most used molecular scaffolds in investigations for the artificial reproduction [19–22] of the aforementioned biological events due to their synthetic accessibility and similar electronic properties (e.g. excitation energies, quantum yields and electron transfer properties). Thus, ever since the first crystal structure of porphyrin was obtained [23], the knowledge of the chemical and physical properties of such macrocyclic structures has grown rapidly, fuelling the expansion of research activities focused on the development of new synthetic methodologies [24–26] and on the study of potential applications in optoelectronics [27–33], electrochemistry [34], catalysis [35], molecular recognition [21,36,37], sensors [38,39], data storage [7] and solar cells [19,22,40,41]. The self-assemblies of various porphyrins have been studied both in solution and in the solid state. Recent examples have demonstrated that self-assembled architectures can be engineered at the submicrometer level using non-covalent interactions, such as coordination bonds, hydrogen-bonding and π–π stacking. As an example, Hu et al. [42] recently reported the surfactant-assisted self-assembly of zinc(II) *meso*-tetra(4-pyridyl)porphyrin (**1**) in solution to form uniform sized 1D hollow hexagonal nanoprisms (Fig. 1a) as characterised by X-ray diffraction (XRD), scanning electron microscopy (SEM) and transmission electron microscopy (TEM). The XRD data indicated that the assemblies form *via* the axial coordination of the pyridyl groups to the zinc metal centres. The size of the nanoprisms was adjustable in length and aspect ratio (longitudinal/lateral dimension) by altering the stoichiometric ratio of molecule **1** over the cetyltrimethylammonium bromide surfactant. Also, following the evaporation of the solvent, the nanoprisms self-organised into ordered 3D stacks (Fig. 1b). This superstructure formation was attributed to the good monodispersity and regular geometric shape of the nanoprisms. Schematic illustrations of self-assembly processes of the nanoprism and the superstructure are shown in Fig. 1c

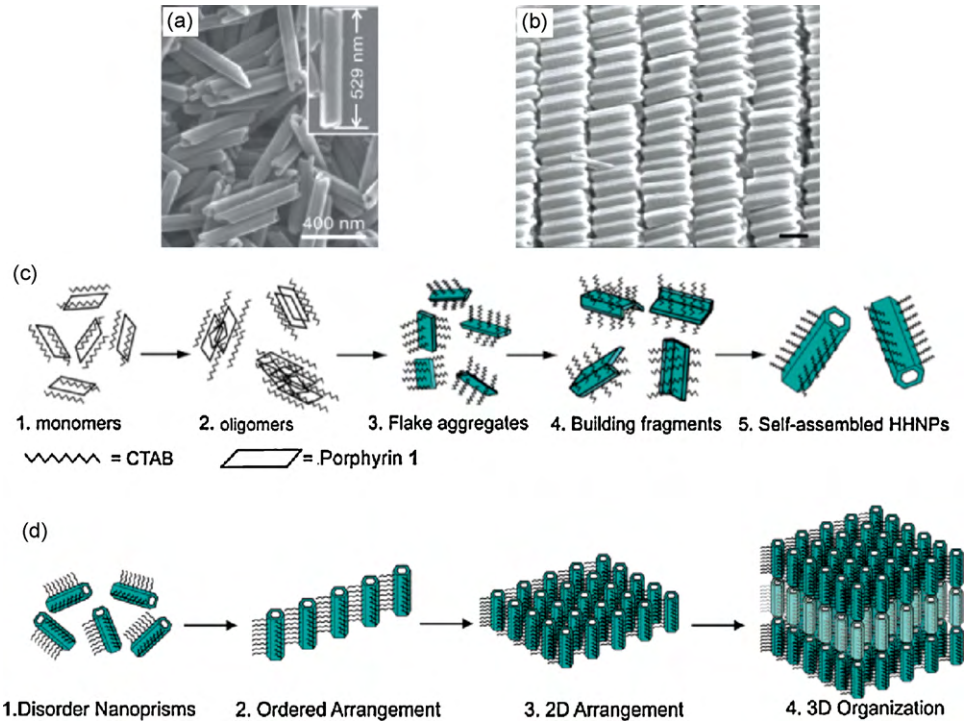

Fig. 1. (a) SEM image of the hollow hexagonal nanoprisms formed by the CTAB-assisted self-assembly of porphyrin **1**. The inset shows the average length (529 nm) of the sized nanoprisms. (b) SEM image of the horizontal arrangement of the superstructure formed by the nanoprisms upon evaporation of the solvent. (c) Schematic representation of the formation of the nanoprism assemblies. (d) Schematic representation of the formation of the superstructure.
This figure was reproduced from reference [42], with the permission of the copyright holders.

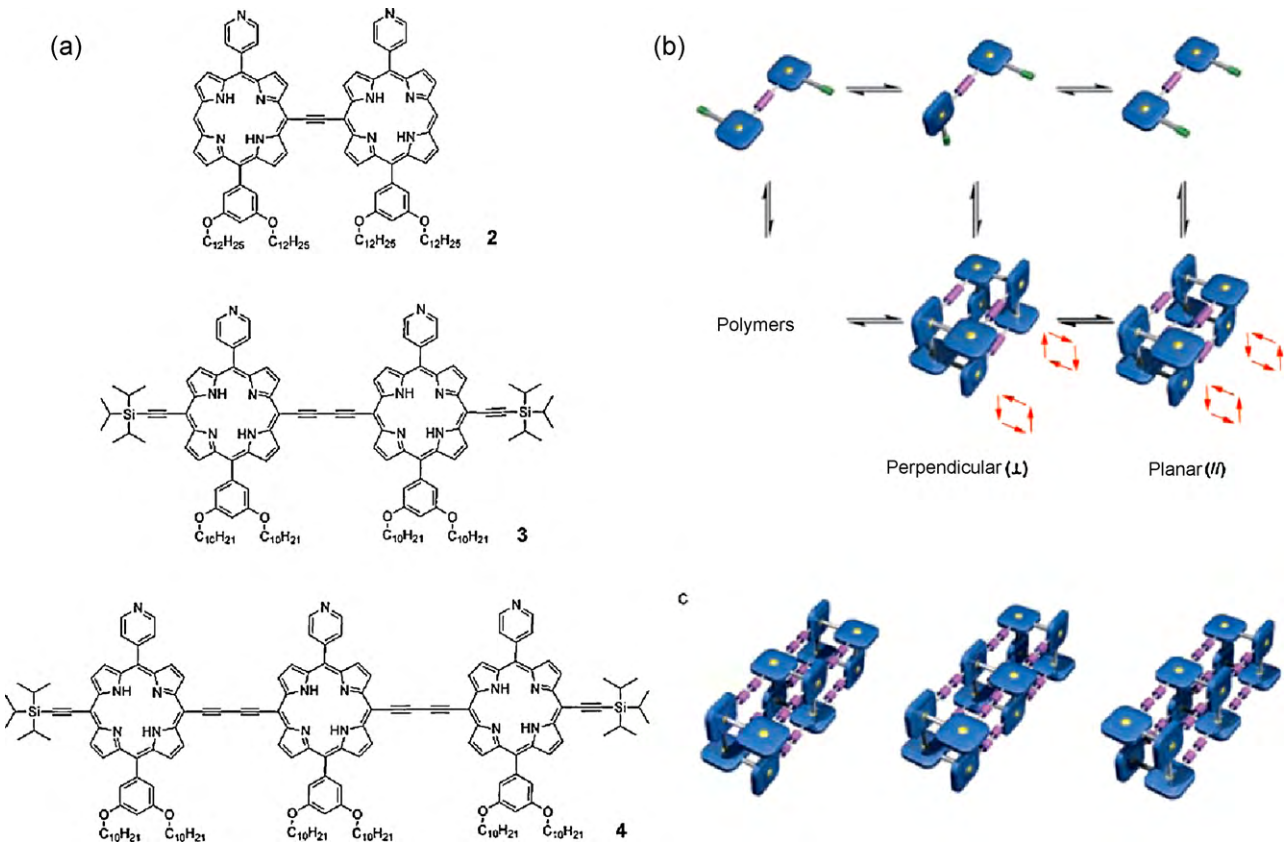

Fig. 2. (a) Molecular structures of the mono- and di-alkynylene-bridged bis- or tris-porphyrin molecules porphyrins investigated. (b) Schematic representation of the possible supramolecular assemblies that can be formed by **2** and **3**, *i.e.*, perpendicular or planar conformations. (c) Schematic representation of the possible supramolecular assemblies that can be formed by **4**, *i.e.*, perpendicular, mixed perpendicular with planar, or planar conformations.
This figure was reproduced from reference [43], with the permission of the copyright holders.

and d, respectively. Using the same interaction motif, *i.e.* pyridyl groups coordinated to porphyrin zinc metal centres, it was shown by Tsuda et al. [43] that box-shaped cyclic tetramers could be self-assembled in solution using various mono- and di-alkynylene-bridged bis- or tris-porphyrin molecules (**2**–**4**, Fig. 2a–c). The rotational freedom around the acetylene bonds permits the formation of planar and perpendicular conformations upon coordinative cyclooligomerization, however the former is enthalpically favoured because the π-conjugation in the planar conformation is extended. Indeed, the planar conformation was observed for porphyrin **2**, but not for molecules **3** and **4**, which preferred to adopt the perpendicular conformation due the efficient annulment of the pyridyl dipole moments in the perpendicular conformer.

In two related papers published by Kobuke and co-workers, coordinative bonding between the N atom of imidazoyl substituents and Zn(II) metal centres of neighbouring porphyrins could also be exploited to yield linear [44] and cyclic [45] arrays in solution (see also similar work in Section 2).

In the context of molecular assemblies at the solid state, Goldberg [46] presented, in 2005, a detailed survey of studies that describe the design of porphyrin modules and their use in crystal engineering. An example of a very versatile scaffold is tetra(4-carboxyphenyl)porphyrin (**5**), which forms open arrays that resemble molecular sieves or zeolite materials displaying an unprecedented long-term stability at ambient conditions.

Despite these achievements, a technical impediment towards the exploitation of such porphyrin-based nanoscale systems in molecular devices is that they cannot be directly addressed in solution or in a crystal, as they must be able to show durability and functionality under the extreme conditions that are normally used in operating practical devices [47]. These problems have started to be addressed by depositing the functional organic materials on surfaces, and subsequently using Scanning Probe Microscopies (SPM), and in particular Scanning Tunnelling Microscopy techniques (STM) [48,49], to perform their nanoscale characterisation. Despite the large scientific production describing the organisation of molecules on metallic surfaces [50–64], the development of hybrid functional devices in which surfaces are modified with functional molecular assemblies [53,65–67] is believed to be the key to bringing forth applications in many fields ranging from electronics [68–78] to nanomedicine [79,80]. In this respect, porous two-dimensional (2D) networks are of particular interest since the array's cavities (potentially controllable both in size and shape) can be used to host functional molecules that can be remotely controlled, bringing functionality and device-like features at the nanoscale level to the structural material.

In this review, a perspective of the recent developments related to supramolecular assemblies of porphyrin derivatives on surfaces will be illustrated using key examples that have recently appeared in the literature. The discussion will unroll through three sections. The first will treat discrete non-covalent multi-porphyrin assemblies on surfaces prepared and studied under ultra-high vacuum (UHV) conditions. Section 2 will tackle bi-dimensional porphyrin-based netwroks (investigated by STM at the liquid–solid interface and under UHV conditions). Finally, the last section will deal with porphyrin assemblies featuring a 3rd dimension. Specifically, examples describing three-dimensional structures displaying functional properties will be described.

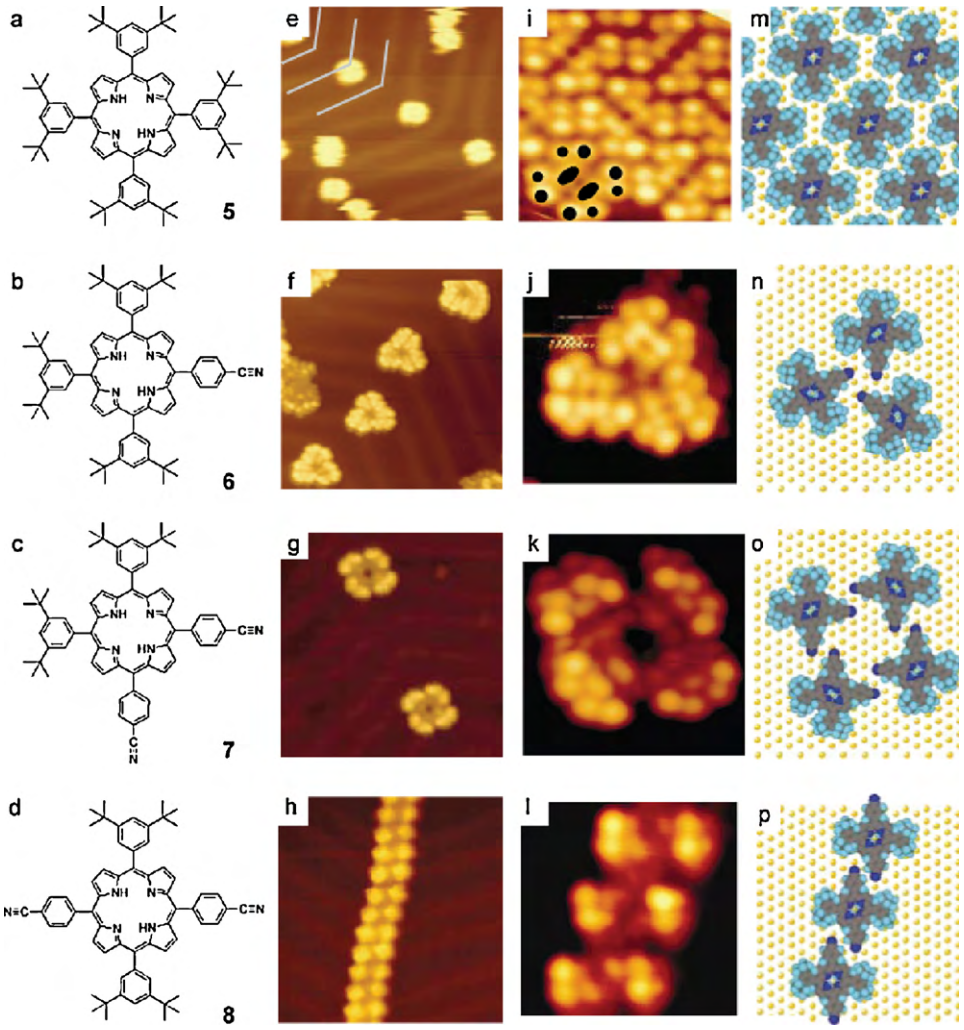

Fig. 3. (a–d) Molecular structures of the investigated porphyrins. (e–h) STM images (20 nm × 20 nm) taken at 63 K of the supramolecular assemblies formed by **5**–**8**. The herringbone patterns of Au(1 1 1) are shown in (e). (i–l) High resolution STM images (5.3 nm × 5.3 nm) of the porphyrin assemblies. The black dots in (i) represent a single a porphyrin molecule consisting of two oblong protrusions (porphyrin core) surrounded by four paired lobes (*t*-butyl groups). (m–p) Molecular models of the observed assemblies.
This figure was reproduced from reference [81], with the permission of the copyright holders.

2. Discrete multi-porphyrin assemblies

The first examples of discrete supramolecular assemblies of porphyrin derivatives on surfaces was published by Yokoyama et al. [81] The assemblies of four porphyrins (**5**–**8**, Fig. 3a–d) were investigated on a Au(1 1 1) surface under UHV conditions using low temperature (63 K) STM to determine the influence of cyanophenyl groups on the aggregation.

Three types of intermolecular interaction have been invoked between the cyanophenyl groups (Fig. 4) [81,82]: antiparallel dipolar C≡N···C≡N interactions; trimeric bonding which involves the cyano group and positive polarized hydrogen atoms in the ortho position to the cyano group, C≡N···H–C_{ortho}; and a H-bonding type interaction between the cyano groups and a sp^2 carbon on the phenyl ring which is substantially weaker than a classic H-bond C≡N···H–$C_{sp}{}^2$ bond. Porphyrin **5**, which does not bear any cyanophenyl groups, did not aggregate at low coverage (Fig. 3e), however, upon further deposition, a close-packed arrangement of the molecules could be observed (Fig. 3i and m). Porphyrin **6**, with a single cyanophenyl group formed trimers upon deposition onto the Au surface (Fig. 3f, j and n), as a consequence of the cyclic configuration assumed by the cyanophenyl groups' trimeric bonding interactions. In order to probe the system further, two other porphyrins were synthesised bearing two cyanophenyl substituents: *cis*-like and *trans*-like isomers **7** and **8**, respectively. Molecule **7** forms a supramolecular tetramer on the surface (Fig. 3g, k and o), guided by the antiparallel dipolar interactions of the adjacent cyano groups. In contrast with this, *trans*-like isomer **8** forms supramolecular wires with lengths over 100 nm (Fig. 3h, l and p). In all these assemblies, the Au(1 1 1) surface does not only act as a substrate, but also interacts with the porphyrins guiding the initiation positions of the discrete assemblies and supramolecular wires; the Au(1 1 1) surface is characterised by 'herringbone' patterns [83] (see the reconstructed pattern shown in Fig. 3e), and in all cases, the porphyrins were mainly located at the apices of the pattern since these are ideal nucleation points.

In a recent publication, Diederich and co-workers [82] expand on the work of Yokoyama et al. reporting the self-assembly of two bis-cyanobiphenyl porphyrin derivatives (bearing two 4′-cyanobiphenyl and two 3,5-di(*tert*-butyl)phenyl substituents in *cis*-like **9** and *trans*-like **10** orientations, respectively, Fig. 5a) on a Cu(1 1 1) surface under UHV conditions. Surprisingly, in the case of the *cis*-like isomer, various discrete supramolecularly assembled macrocyclic oligomers were observed, ranging from dimers to hexamers (Fig. 5c–h). This large variety in the observed assemblies has been attributed to two facts: (a) the presence of

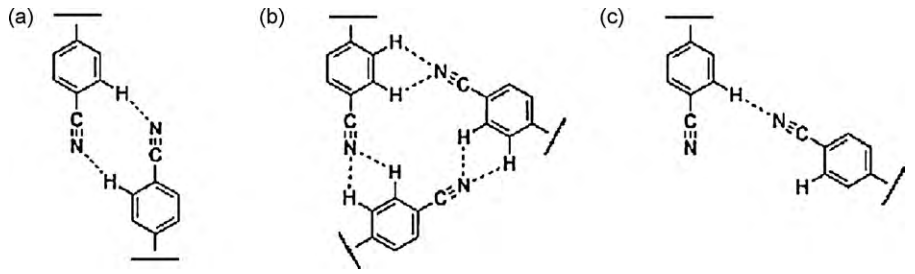

Fig. 4. Typical interactions of cyanophenyl groups: (a) antiparallel dipole–dipole, (b) trimeric bonding, and (c) hydrogen bond-type association. This figure was reproduced from references [81,82], with the permission of the copyright holders.

contributions other than dipolar bonding interactions which direct the formation of other favourable geometries and (b) Cu(1 1 1) surfaces has a stronger interaction with large aromatic systems in comparison to Au(1 1 1), thus the porphyrins adsorbed on the surface tend to align to principle directions of the substrate, altering the balance in strength between the adsorbate–adsorbate and adsorbate–substrate interactions. Despite the large variety of the observed architectures, the most common assemblies were trimers and tetramers. In the trimeric species (Fig. 5d), each of the three porphyrins has its central axis rotated of 120° with respect to the next, and thus each one is favourably aligned to the principle directions of the Cu(1 1 1) surface. As no bending of the cyanobiphenyl moieties is apparent in the STM images and the structural alignment between neighbouring cyano groups is estimated at an angle of 150°, it means that the interaction is a hybrid between antiparallel dipolar and hydrogen-bonding interactions. Two types of tetramers were observed (Fig. 5e and f) due to the fact that porphyrins form conformational enantiomers upon deposition on surfaces. The *meso*-phenyl substituents are rotated away from their preferred perpendicular orientation relative to the porphyrin core, causing a saddle shape to form in the porphyrin core with two opposing pyrrole rings pointing upwards, and the other two pointing downwards. This can occur in two axes (Fig. 5b), leading to type A and type B. One of the tetramers is formed by two type A and two type B porphyrins (Fig. 5e). The interactions of the CN groups in this case are at 180°, the optimal angle for antiparallel dipolar interactions, and furthermore, all the porphyrins are aligned with the Cu(1 1 1) surface axes. In the second type of tetramer (Fig. 5f), the porphyrins are all of the B type, and in order to maintain their alignment on the Cu substrate's axes, the 4′-cyanobiphenyl substituents bend (inwards in two of the porphyrins and outwards in the other two) to be able to intermolecularly interact. Pentamers were also observed (Fig. 5g), but very rarely because the formation does not correctly fit the Cu(1 1 1) lattice nor the 90° angle of the cyano groups of the porphyrins. Hexameric structures conform to the Cu(1 1 1) lattice, however due to the large cavities, they are generally less favoured and very infrequently observed (Fig. 5h). The most interesting result obtained with porphyrin **9** was related to the dimer formation. The bonding interaction for the dimer was expected to be similar to that of the trimeric arrangement, where the CN group of one porphyrin would interact with the phenyl hydrogen atoms of the neighbouring porphyrin macrocycle as this arrangement would conform to the geometry of molecule **9** (Fig. 5c). However, another dimeric system was observed when the assembly was annealed above 150 °C, causing a distortion of the 4′-cyanobiphenyl substituents, closing to approximately 60°. This extreme distortion is thought to be caused, firstly, by the aforementioned Cu-substrate-induced saddle shape of the tetrapyrrolic core permitting the *meso*-substiutents to move laterally, an effect that is even more pronounced at elevated temperatures; and secondly, and more significantly, the elevated temperatures allows for the mobilisation of Cu adatoms from the Cu step edges making them available for the coordination of two cyano groups, and hence the formation of dimers as shown in Fig. 5i–k. The number of such dimers increased further upon heating to 200 °C. In the case of *trans*-enantiomer, **10**, deposition on the Cu(1 1 1) surface at low coverages led to linear chains formed by the antiparallel dipolar interactions of the cyanophenyl moieties (Fig. 5l). In another study, using a related mono-cyanophenyl-functionalised porphyrin, Diederich and co-workers [84] have shown that it is possible to assemble molecular wires over 250 nm in length on insulating surfaces such as potassium bromide. The porphyrin molecules form wires at the step edges of the KBr surface and do not lie flat on the surface due to two interactions: inter-porphyrin π–π stacking and the coordination of the cyanophenyl group to the potassium ions at the apices of the step edges.

Analogous discrete multi-porphyrin assemblies as those in the above example [82] were obtained in parallel in a work involving our own laboratory. Heim et al. [85] investigated the assemblies of three porphyrins bearing pyridyl substituents on a Cu(1 1 1) surface under UHV conditions. As shown in Fig. 6a, one porphyrin bears a single phenyl–acetylene–pyridyl substituent and three 3,5-di(*tert*-butyl)phenyl substituents in the *meso*-positions (**11**). The other two porphyrins are difunctionalised with respect to both types of substituents, bearing the pyridyl moieties in a *cis*-like (**12**) and in a *trans*-like orientation (**13**). Deposition of porphyrin **11** at submonolayer coverage resulted mainly in dimer formation (Fig. 6b and c), with few scattered individual porphyrins present. The dimers are coupled in an antiparallel head-on configuration, in which the pyridyl moieties are facing each other. Instead, performing the same deposition on Ag(1 1 1) did not result in dimerisation, but in densely packed islands where the pyridyl groups avoided each other, thus inferring that the Cu(1 1 1) substrate plays a role in the dimer formation. It is suggested that, through careful analysis of theoretically calculated distances compared with the distances obtained experimentally by STM, the most plausible mechanism of dimer formation is the coordination of the pyridyl groups with Cu adatoms originating from the substrate resulting in a pyridyl–Cu–pyridyl motif. This Cu–pyridyl coordination interaction has been studied in detail by Barth and co-workers using a tetrapyridyl-porphyrin on a Cu(1 1 1) substrate [86]. The coordination brings the H atoms of neighbouring pyridyl groups in close proximity causing steric repulsions, consequently preventing a trimeric coordination from forming as in the case of the cyanophenyl-bearing porphyrin. Furthermore, this repulsion prevents the strong deviations from the optimal 180° angle of the head-on configuration. Although the 180° angle is required for interaction, the phenyl–acetylene–pyridyl functions display some conformation flexibility allowing for some lateral bending. This accounts for the fact that the axis connecting the two porphyrins in the dimeric species does not always follow the direction of atomic lattice of the underlying Cu(1 1 1) substrate, but it can vary with an angle of up to ±15° from it. Deposition of *cis*-dipyridyl porphyrin **12**, on the Cu(1 1 1) surface resulted in various discrete supramolecular

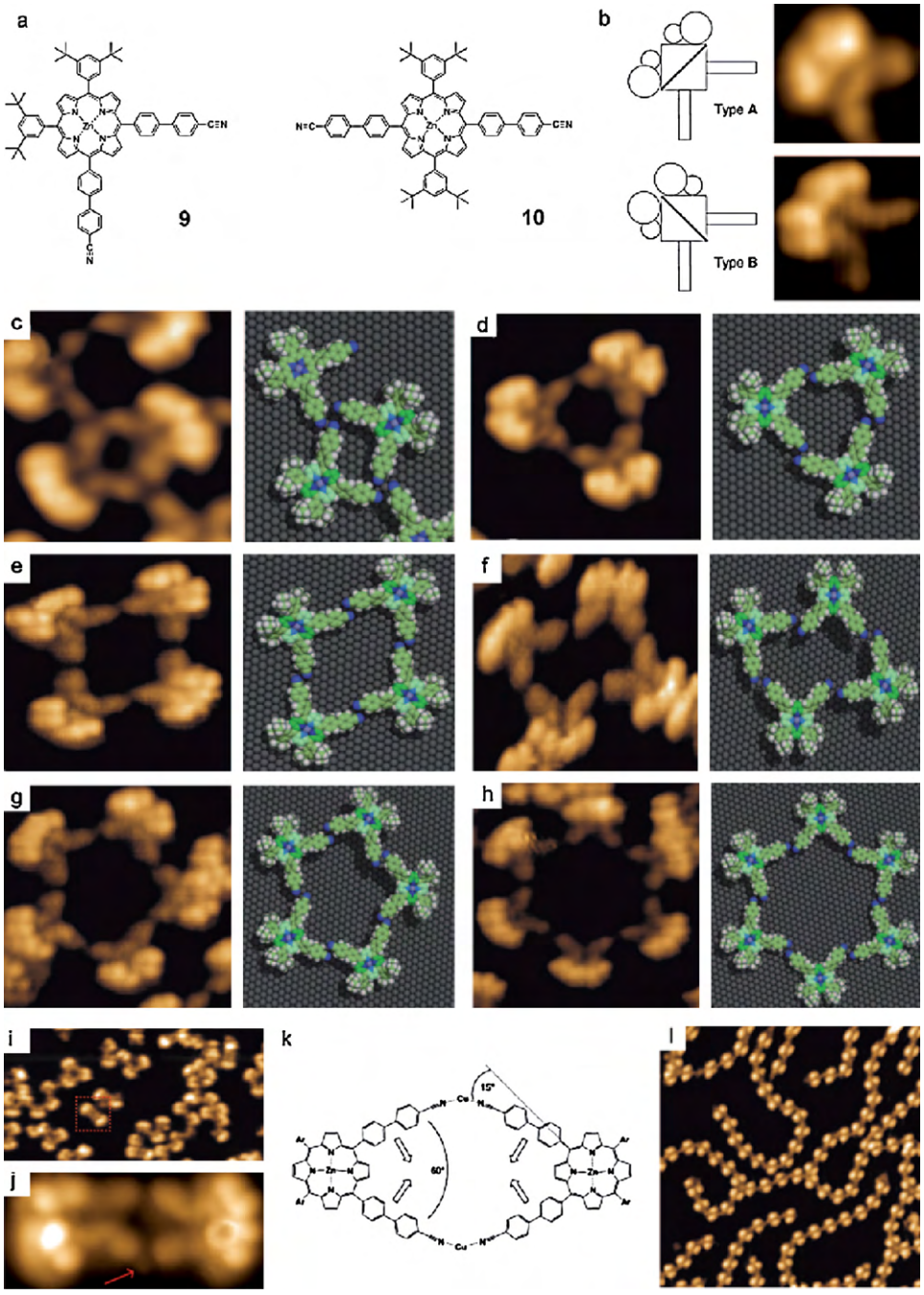

Fig. 5. (a) Molecular structures of porphyrins **9** and **10**. (b) Conformational isomers, type A and B of **9**. (c–h) High resolution STM images with the corresponding molecular models of the various self-assembled macrocyclic oligomers: (c) dimer (5.0 nm × 5.0 nm); (d) all type A trimer (6.3 nm × 6.3 nm); (e) mixed type tetramer (6.4 nm × 6.4 nm); (f) all type B tetramer (6.2 nm × 6.2 nm); (g) pentamer (7.6 nm × 7.6 nm); (h) hexamer (8.2 nm × 8.2 nm). (i) STM image (50 nm × 26 nm) for submonolayer coverage of **9** on Cu(1 1 1) annealed at 150 °C. The dimer marked by a square is enlarged in (j). (j) High resolution STM image (5.5 nm × 2.5 nm) of a dimer. (k) The proposed model for the dimer showing that the 4′-cyanobiphenyl groups bend together by ∼15° to enable coordination with Cu atoms. Ar = 3,5-di(*tert*-butyl)phenyl. (l) STM image showing the branched linear chains formed at low coverages by **10** on Cu(1 1 1).
This figure was reproduced from reference [82], with the permission of the copyright holders.

assemblies (Fig. 6d). Triangular and rhombic shaped assemblies were mainly observed. The trimeric assembly (Fig. 6e) dominated at low coverage, whereas, the tetrameric species dominated at higher coverages (Fig. 6f), with the pentameric (Fig. 6g) and hexameric assemblies (Fig. 6h) also appearing at the increased coverages. This tendency demonstrates that the spontaneous self-assembly and the structural properties of the architectures depends on a combination of the pyridyl–pyridyl interactions, the conformational flexibility of the molecular modules and also the influence of the Cu substrate (as also shown by Fendt et al. [82]). Surprisingly, perpendicular angles between the substituents were very rarely observed on the surface, as the 3,5-di(*tert*-butyl)phenyl substituents generally have angles of 60° (type A porphyrin) or 120° (type B porphyrin) with respect to each other, and the pyridyl substituents were at opening angles of 80 ± 5° (type A) or 100 ± 5° (type B). In the triangular assembly all the porphyrin units were of type A and due to the substrate atomic lattice, the triangles could only be found in two orientations on the surface, which followed the Cu orientations (indicated

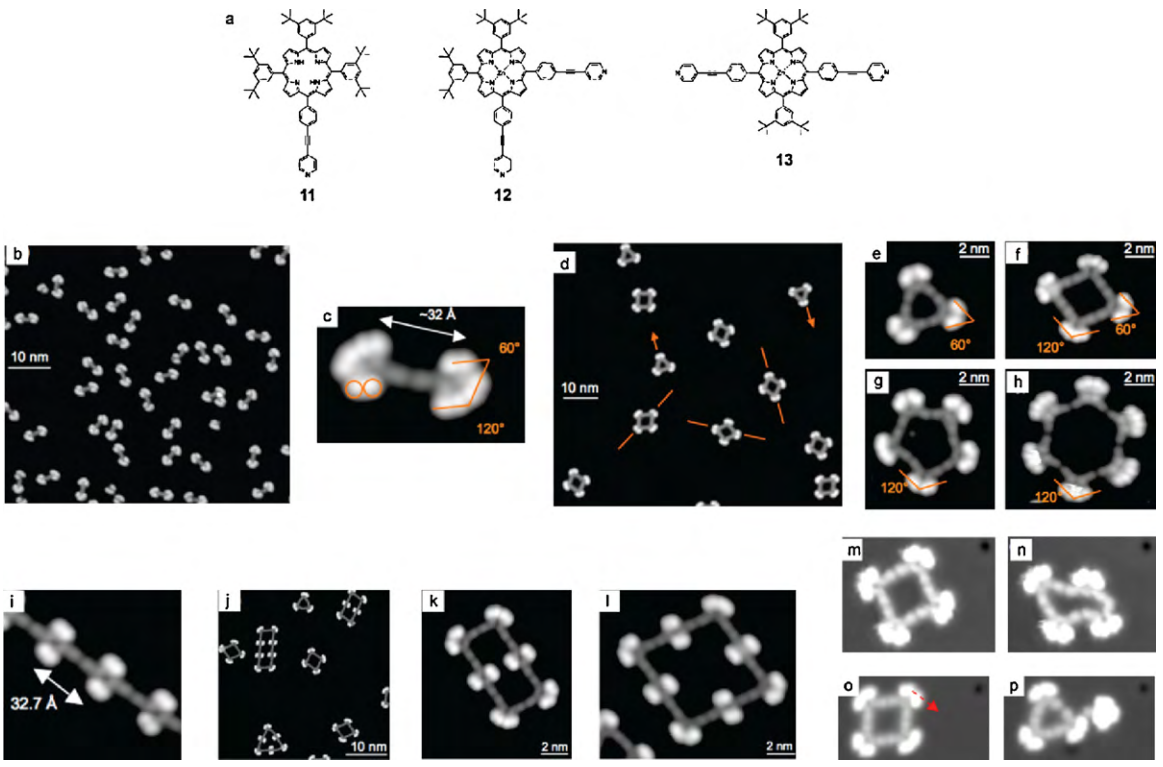

Fig. 6. (a) Molecular structures of pyridyl-substituted porphyrins **11**–**13**. (b) STM image of the self-assembled dimers formed by porphyrin **11** on a Cu(1 1 1) surface. (c) Detailed view of a single dimer. Each of the bright double lobes (circles) represents a *t*-Bu_2Ph group. The head-on aligned pyridyl-substituents can also be seen in grey. (d) STM image of the triangular and rhombic supramolecules formed by porphyrin **12**. The lines and arrows mark the azimuthal orientations of the assemblies. (e–h) Detailed STM images of the supramolecular cycles $(\mathbf{12})_n$ (e, $n=3$; f, $n=4$; g, $n=5$; h, $n=6$). The opening angles of the *t*-Bu_2Ph groups are indicated. (i) STM image of the 1D molecular wires formed upon deposition of **13** on Cu(1 1 1). (j) STM image showing the coexistance of homomolecular assemblies and bicomponent rhombic and triangular architectures formed following a mixed deposition of **12** and **13**. (k and l) Detailed view of the bicomponent cyclic assemblies. (m–p) Molecular manipulation experiment where the STM tip using low tunnelling resistance was used to distort a tetramer of **12** without break the intermolecular bonds (m–n) and also to extract one molecule converting a tetramer into a trimer (o–p).
This figure was reproduced from reference [85], with the permission of the copyright holders.

by arrows in Fig. 6d), and were at 180° with respect to each other. The tetrameric macrocycles involved two A-type and two B-type porphyrins resulting in rhombic shapes, found in the three orientations on the surface respecting the Cu atomic lattice directions. The pentameric and hexameric assemblies were made up of B-type porphyrins only. In the case of *trans*-substituted porphyrin **13**, deposition resulted in extended chains (Fig. 6i) as expected. Further investigations involving the deposition of a bicomponent mixture of porphyrins **12** and **13** (in 3.6:1 ratio), led to the formation of various large unprecedented cyclic structures incorporating both porphyrins (Fig. 6k and l). Further to these results, the work also demonstrated that the assemblies could be singularly manipulated using the STM tip (Fig. 6m–p), displaying unprecedented flexibility and robustness.

Using a different approach to form discrete porphyrin assemblies on surfaces, Kobuke and co-workers [87] were able to deposit preformed coordination assembled porphyrin macrocycles reinforced with covalent links using pulse injection onto a Au(1 1 1) surface under UHV conditions. Ferrocene-bridged trisporphyrin (**14**) self-assembles in solution to form macrocycles (**15**) ranging from dimers to decamers due to the coordination of the imidazolyl substituents with the Zn-centre of the adjacent porphyrin core (Fig. 7a) [88]. The supramolecular cycles formed were further reinforced using a ring closing metathesis reaction using Grubbs' catalyst resulting in a bridge between the *meso*-positions of the coordinated porphyrins (**16**). The resultant porphyrin array was deposited onto a Au(1 1 1) surface and was subsequently studied by STM revealing the presence of circular shapes made up of bright spots corresponding to the number of constitutional units in the array. Images were obtained for the pentamer and decamer, which corresponded in size to the calculated values (Fig. 7b and c and d and e respectively). Such circular shapes were not observed without the covalent reinforcement, that is, with the macrocycles prior to the metathesis reaction (**15**), indicating that complementary coordination alone is not sufficient to maintain the assembled array on a metal substrate.

Regarding the strength of the interaction, H-bonded and metallo-organic coordinated networks on surfaces can be classified midway between the weak non-covalent interactions like van der Waals, π–π or dipole–dipole and the robust covalent polymers, which are thought to display the required stability for nanotechnological applications [89]. As a result, the construction of covalently bonded architectures on surfaces (also called surface covalent organic framestudies, SCOFs) apparently displaying higher stabilities towards external manipulation *stimuli* has also been attempted recently. One of the first examples of a covalently bonded 2D porous network on a surface was published by Grill et al. [90] *meso*-Substituted porphyrins bearing varying numbers of *para*-bromophenyl moieties were used to form arrays on Au(1 1 1) surfaces under UHV conditions. Covalent bonds at predetermined points were formed by thermal dissociation at temperatures above 590 K. The thermal dissociation reactions were carried out by either heating the porphyrin molecules in the evaporator or by heating them on the surface following their sublimation. In both cases, intermolecular coupling between the monomeric species resulted (Fig. 8). Control experiments at lower temperature (sublimation at 550 K) using the tetra(4-bromophenyl)porphyrin units (**17**), led to islands (up to 100 nm in diameter) of highly ordered

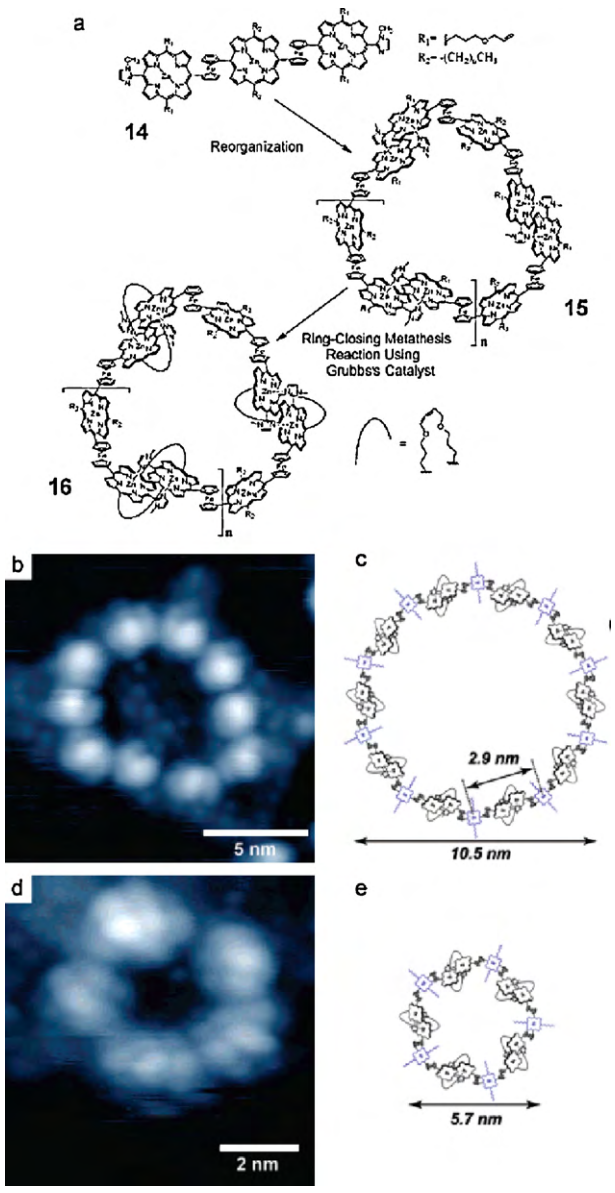

Fig. 7. (a) Preparation scheme of a series of supramolecular macrocycles (**15**) using trimeric porphyrin precursor (**14**) via the coordination interaction through imidazolyl moieties and the Zn(II) metal centre of an adjacent porphyrin core. Covalent linking was performed by a ring-closing metathesis catalysed by a Grubbs-like catalyst of the allyl substituents at *meso*-positions. (b–d) UHV-STM images of **16**($_{\mathbf{10mer}}$) (b) and **16**($_{\mathbf{5mer}}$) (d) on Au(1 1 1) at −196 °C. The corresponding schematic structures are shown aside the STM images (c and e).
This figure was reproduced from reference [87], with the permission of the copyright holders.

close-packed arrays formed, as shown in Fig. 8a. Various nanoarchitectures were formed in a controlled manner upon thermal activation of the Br functional groups of the mono-, di-, and tetrabromo-substituted tetra(phenyl)porphyrins (TPPs) **17**, **18** and **19**, respectively (Fig. 8b–d). As expected, the mono-bromo-substituted porphyrin **17**, formed dimers upon activation of the reactive sites (Fig. 8b). Long linear chains were formed following the thermal activation of *trans*-di-bromophenyl porphyrin **18**, whereas tetrabromophenyl porphyrin **19** formed 2D networks.

In contrast to supramolecular architectures, covalent assemblies often incorporate unchangeable defects, thus resulting in nanostructures with limited periodicity. This does not happen with supramolecular networks, in which the strength, reversibility and lability of the non-covalent bonding interactions are such that periodic nanostructured materials can be easily prepared. In addition, covalent assemblies are often constrained to a very peculiar chemical reaction, thus displaying a limited applicability and versatility.

3. Bi-dimensional porphyrin networks

3.1. Porphyrin architectures at the liquid–solid interface

The development of high quality films of functional molecules such as porphyrins and/or phthalocyanines on the nanoscale size that function in aqueous conditions is important for the engineering of biocompatible materials for fuel cells applications. In 2003, Itaya and co-workers developed a technique that enabled the deposition and investigation of adlayers of hydrophobic porphyrins, e.g. Co(II) tetraphenylporphyrin (**20**) in electrochemical and STM cells containing aqueous media [91]. The general method involves immersing single crystal electrodes (usually Au(1 1 1) electrodes) into benzene solutions of the relevant porphyrin, rinsing with ultrapure water and transfer into the electrochemical or STM cell (in 0.1 M $HClO_4$). Since this first report, numerous papers have appeared in the literature investigating various types of such porphyrin adlayers and thus only two representative examples will be illustrated in further detail. In the first example, Itaya and co-workers prepared mixed adlayers of Cu(II) octaethylporphyrin (CuOEP, **21**, Fig. 9a) and Co(II) phthalocyanine (CoPc, **22**, Fig. 9a) on a Au(1 1 1) surface by immersing the substrate in a benzene solution containing the two molecules [92]. Different assemblies were observed depending on the immersion time. Three durations of immersion were investigated, 4, 6 and 20 min (Fig. 9b–g). The adlayer at the immersion time of 4 min was composed of an approximately 1:1 concentration of both types of molecules, and consisted of both well-ordered and disordered areas, with the well-ordered areas forming due to the hexagonally packed CuOEP molecules (Fig. 9b and e). The two types of molecules can be distinguished in the STM images relatively easily since the Co ions appear as bright spots due to the strong current that results from orbital-mediated tunnelling through the half-filled d_{z^2} orbitals. The Cu ions on the other hand appear as dark spots since they do not mediate the tunnelling current. Notably, the CuOEP adlayers form much faster than the CoPc adlayers on Au(1 1 1) due to the stronger interaction between CuOEP molecules compared to the interaction between CoPc molecules. However, extending the immersion time leads to the displacement of CuOEP by CoPc molecules. In fact, after 6 min of immersion, two domains appear (A and B in Fig. 9c and f) both consisting of highly ordered 2D arrays composed of alternating molecular rows of CuOEP (dark) and CoPc (bright). Extending the immersion time to 20 min led to the complete displacement of CuOEP by CoPc molecules so that the entire surface was covered by highly ordered arrays of CoPc units only (Fig. 9d and g). This displacement phenomenon suggests that the assembly of the CuOEP is kinetically favoured whereas the assembly of the CoPc is thermodynamically more stable. Further to the control of the adlayer assembly by immersion time, the structure has also been tuned by the electrode potential. Commencing from the alternating assembly obtained at 6 min immersion time and 0.85 V *vs* RHE (reversible hydrogen electrode) in 0.1 M $HClO_4$ (Fig. 9h), potential stepping to 0.6 V, 0.35 V and back to 0.85 V resulted in phase separated domains. At 0.6 V the ordered domains became smaller in size, being replaced mainly with dark regions of CuOEP assemblies, indicating that 2D organisation of CuOEP molecules is more stable than that of CoPc (Fig. 9i). At 0.35 V, the molecules became highly mobile, thus a blurry STM image was obtained (Fig. 9j), however upon returning the potential to 0.85 V separated domains of the two molecules had formed with bright areas consisting of disordered CoPc molecules and dark areas consisting of hexagonally arranged CuOEP units (Fig. 9k). In another attempt to reorder the

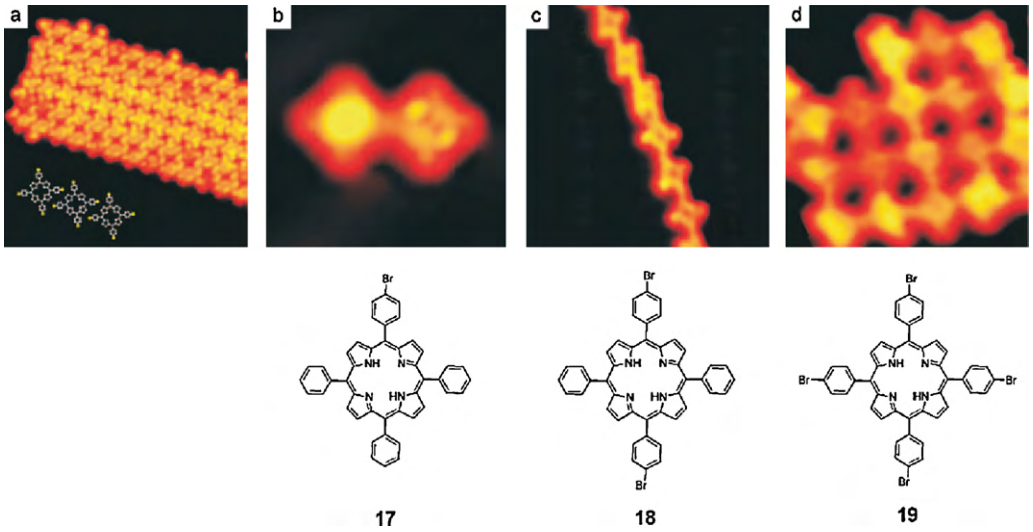

Fig. 8. (a) STM image (20 nm × 20 nm) of islands formed by unactivated porphyrin **19** on Au(1 1 1) after sublimation at 550 K; (b–d) results obtained after the activation of bromophenyl porphyrins **17**, **18** and **19**, respectively. Sizes (b) 5 nm × 5 nm, (c) 10 nm × 10 nm, (d) 8.5 nm × 8.5 nm.
This figure was reproduced from reference [90], with the permission of the copyright holders.

domain sizes and composition, the potential was changed from 0.8 V to 0.45 V gradually with a scan rate of 10 mV s^{-1}. During this potential manipulation, the alternate packing of CuOEP and CoPc disappeared, giving way to arrays of bright CoPc domains with a square lattice and dark CuOEP domains with quasi-hexagonal packing (Fig. 9l).

In the second example [93], very similar molecules, zinc(II) phthalocyanine (ZnPc, **23**) and zinc(II) octaethylporphyrin (ZnOEP, **24**) were used. In this work, 2D alternate arrays consisting of ZnPc and ZnOEP were prepared on Au(1 1 1) electrodes, and were then used to host C_{60} molecules. The bicomponent arrays of ZnPc and ZnOEP were prepared in an analogous manner as described above and were initially investigated at a potential of 0.8 V *vs* RHE. With the concentration of both molecules being roughly equal, three domains were observed on the surface (Fig. 10a). Domain I consisted of well-ordered mixed assemblies of ZnPc and ZnOEP. In domain II pure ZnOEP was assembled, and domain III was compositionally disordered. Domain I was predominant under the employed experimental conditions and was particularly interesting since the self-assembly was 'chessboard'-like in appearance with alternating ZnPc (bright, propeller-shaped) and ZnOEP (dark, ring-shaped) molecules (Fig. 10b and c). Domains I and II were stable to potential manipulations from 0.85 to 0.15 V. Domain III, however, became more ordered as the potential was manipulated. At 0.6 V, alternately arranged molecular rows appeared (Fig. 10d–f), which were stable until a potential of 0.15 V, where the images became unclear, but appeared to consist of solely ZnOEP molecular assemblies. Raising the potential to 0.2 V resulted in separated domains of ZnPc and ZnOEP, as it was seen in the previous work with molecules **21** and **22**. This observation suggested that the ZnPc molecules could be selectively desorbed from the surface. In order to examine the relationship between chemical structure and the bimolecular array formed, a mixture of ZnOEP with zinc(II) tetraphenylporphyrin (ZnTPP, **25**) was also investigated and resulted in nanohexagon structures with eight ZnTPP surrounding each ZnOEP molecule. This assembly was stable to potential manipulations down to 0.1 V, possibly due to stabilising π–π interactions between neighbouring phenyl groups. This observation, along with the stability of the domains I and II in the ZnPc/ZnOEP assembly, infers that the phase separation of a bicomponent system is dependant on the strength of the intermolecular interactions in the 2D arrays formed. The assembly between ZnPc and ZnOEP was further used to nest C_{60} molecules. Bright spots representing C_{60} were only observed in domain I (upper part of Fig. 10g). The C_{60} molecules were located at the gaps between ZnPc molecules exposing the Au substrate (Fig. 10h and i). It is thought that the electronic charge distribution of these exposed Au sites is enhanced due to the π-donating capacity of the ZnPc and ZnOEP molecules in the vicinity, consequently favouring the preferential fullerene adsorption. However, when further C_{60} molecules were deposited on the bicomponent chessboard, two changes occurred. Disturbance of the adlayer by the C_{60} molecules was observed and also, in domains where the adlayer remained intact, the fullerenes assembled upon the chessboard assuming a square shaped assembly (Fig. 10j–l). The C_{60} molecules in this case could easily be removed from the assembly by the STM tip indicating that the interaction between the C_{60} and the bimolecular chessboard is relatively weak.

Feringa and co-workers have also observed the formation of self-assembled networks of porphyrins at the liquid–solid interface [94]. The classic deposition method for liquid–solid STM measurements was used in this study. A drop of a 0.1 mM solution of 5,10,15,20-*meso*-tetradodecylporphyrin (**26**, Fig. 11a) in *n*-tetradecane was deposited on highly ordered pyrolytic graphite (HOPG), as well as Au(1 1 1) surfaces. The resultant self-assembled networks were observed by STM and compared. Deposition on HOPG resulted in a highly ordered monolayer of **26** (Fig. 11b), where the bright spots (diameter ≈ 0.6 nm) correspond to the porphyrin cores lying flat on the surface. Each porphyrin in the 2D network (unit cell: $a = 1.4 \pm 0.1$ nm, $b = 1.7 \pm 0.1$ nm, $\gamma = 108 \pm 1°$) occupied an average area of 2.2 ± 0.1 nm^2, which corresponded to the porphyrin heterocycle (~0.8 nm^2) and two dodecyl chains (~0.7 nm^2 each) physisorbed on the surface, therefore they concluded that the two remaining dodecyl chains were pointing away from the surface into the solution. Deposition on the Au(1 1 1), also resulted in highly ordered monolayers of **26** (Fig. 11c and d), however the assembly was not the same as that on HOPG. A network of four-leaf clover shapes (diameter ≈ 0.35 nm) was observed, where each bright lobe corresponded to a pyrrole moiety in the porphyrin macrocycle. The area occupied by each molecule of **26** on the Au(1 1 1) surface was 1.8 ± 0.1 nm^2, which correlates to the physisorbtion of the porphyrin heterocycle (~0.8 nm^2) and a single dodecyl chain (~0.8 nm^2 on Au(1 1 1)), with the remaining alkyl chains pointing away from the surface into the solution. Two different packing modes of porphyin **26** were observed (Fig. 11f and g). In Fig. 11f, in

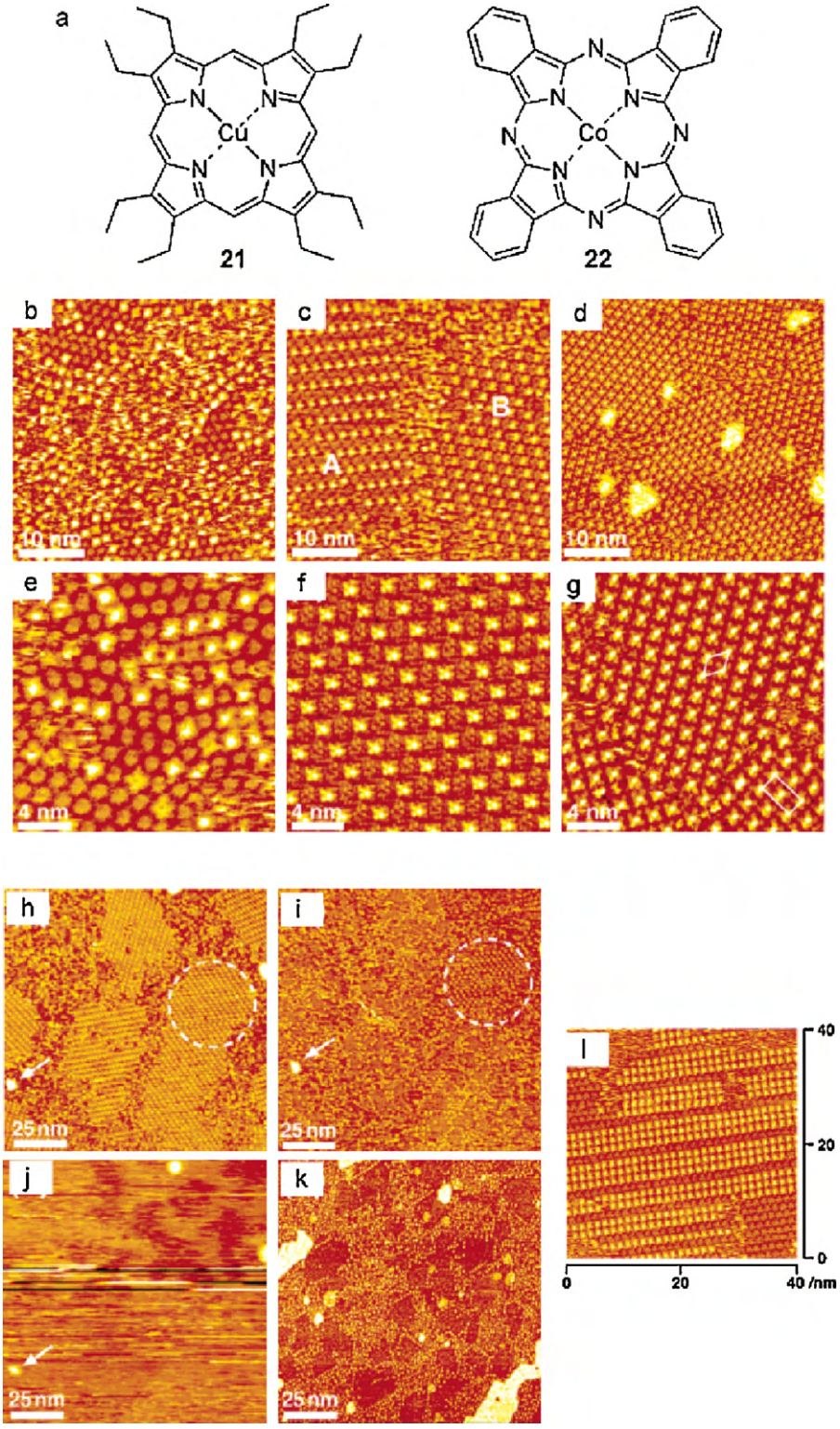

Fig. 9. (a) Molecular structures of the investigated porphyrins, **21** (CuOEP) and **22** (CoPc). (b–g) Typical large-scale (40 nm × 40 nm) and higher resolution (20 nm × 20 nm) STM images, acquired at 0.85 V vs RHE in 0.1 M HClO4, of CuOEP and CoPc binary arrays on Au(1 1 1) prepared by immersion in ~3 μM CuOEP benzene solution saturated with CoPc. The immersion times were 4 min (b and e), 6 min (c and f), and 20 min (d and g), respectively. (h–k) STM images (125 nm × 125 nm) displaying the changes in the self-assembly formed with 6 min immersion upon step-wise potential manipulation: 0.8 V (h), 0.6 V (i), 0.35 V (j), and 0.85 V (k). (l) STM image (40 nm × 40 nm) displaying the changes in the self-assembly formed with 6 min immersion upon gradual potential manipulation from 0.85 V to 0.65 V.
This figure was reproduced from reference [92], with the permission of the copyright holders.

the first packing motif (unit cell: $a = 1.7 \pm 0.1$ nm, $b = 1.1 \pm 0.1$ nm, $\gamma = 105 \pm 1^{\circ}$) all the alkyl chains are aligned along the ⟨1 1 0⟩ axis of the Au(1 1 1) substrate, however the assembly is not perfect, as can bee seen from Fig. 11c, since at random intervals, some of the porphyrin's alkyl chains are aligned to the ⟨1 1 2⟩ axis of Au(1 1 1). The second type of packing (unit cell: $a = 1.5 \pm 0.1$ nm, $b = 2.3 \pm 0.1$ nm, $\gamma = 96 \pm 1^{\circ}$) is shown in Fig. 11g, where the adjacent porphyrin's alkyl chains alternate between the ⟨1 1 0⟩ and ⟨1 1 2⟩ axes of the sub-

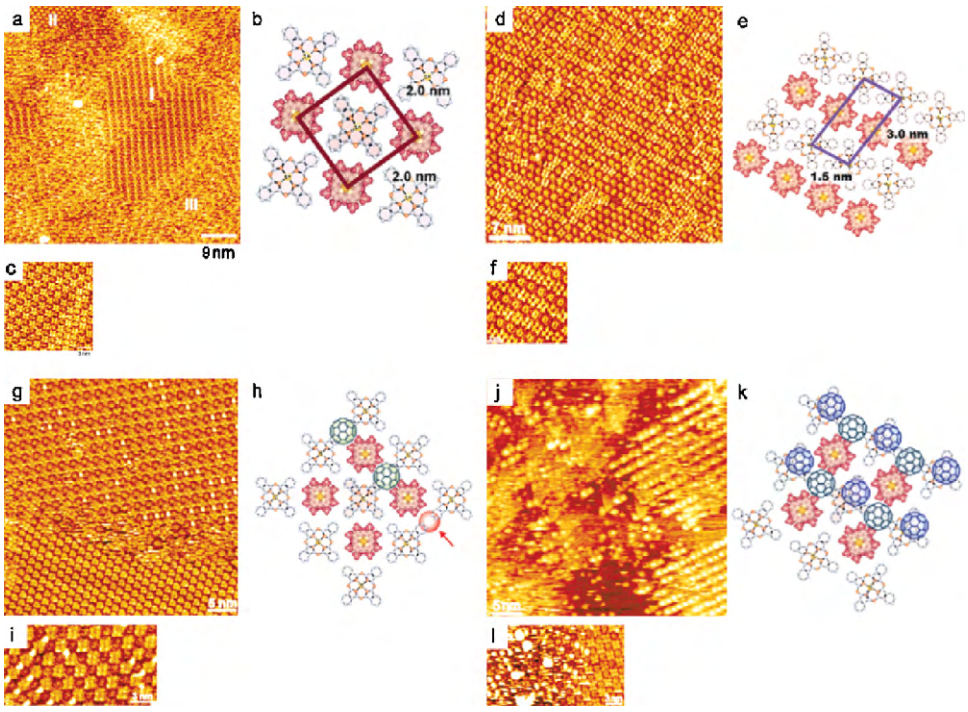

Fig. 10. (a) STM image of the self-assembly of the bimolecular system involving **23** and **24** on Au(1 1 1) at 0.8 V. Three distinct domains are indicated. (b) Proposed model for the bimolecular chessboard shown domain I. (c) High resolution STM image of the bimolecular chessboard (domain I). (d) STM image of the self-assembly of **23** and **24** at 0.6 V. (e) Proposed model for the assembly shown in (d and f). (f) High resolution STM image of the assembly in (d). (g) STM image of C_{60} molecules self-assembled on the bimolecular chessboard array shown in (c). (h) Proposed model for the assembly shown in (g and i). (i) High resolution STM image of the assembly in (g). (j) STM image of the C_{60}-**23**–**24** self-assembly when further C_{60} molecules were introduced. (k) Proposed model for the assembly shown in (j and l). (l) High resolution STM image of the assembly in (j).
This figure was reproduced from reference [93], with the permission of the copyright holders.

strate. The comparison of the two deposition experiments clearly shows that the surface density of molecule **26** on Au(1 1 1) is higher than on HOPG. The authors conclude that the reason for this trend is that a favourable interaction must exist between the Au substrate and the aromatic heterocycle, which causes a conformational distortion of the heterocycle out of planarity. This provides an explanation to why the porphyrin appears as a single bright spot on HOPG and as a four leaf clover shape on Au(1 1 1), with two brighter and two darker lobes (Fig. 11d), suggesting a distortion caused by a coordinative interaction between the macrocyclic nitrogen atoms and the Au surface. This hypothesis was supported by X-ray photoelectron spectroscopy (XPS) experiments, which indicated the presence of three types of nitrogen species in the monolayers, the pyrrolic nitrogen atoms (>NH), free iminic nitrogen atoms (–C=N–), and also coordinated iminic nitrogen atoms.

3.2. Porphyrin architectures under UHV conditions

One of the first depositions of a porphyrin derivative onto surfaces under UHV conditions was carried out by Jung et al. [95] The study involved investigating Cu(II) tetra(3,5-di-*tert*-butylphenyl)porphyrin (**27**, Fig. 12a) on three different surfaces,

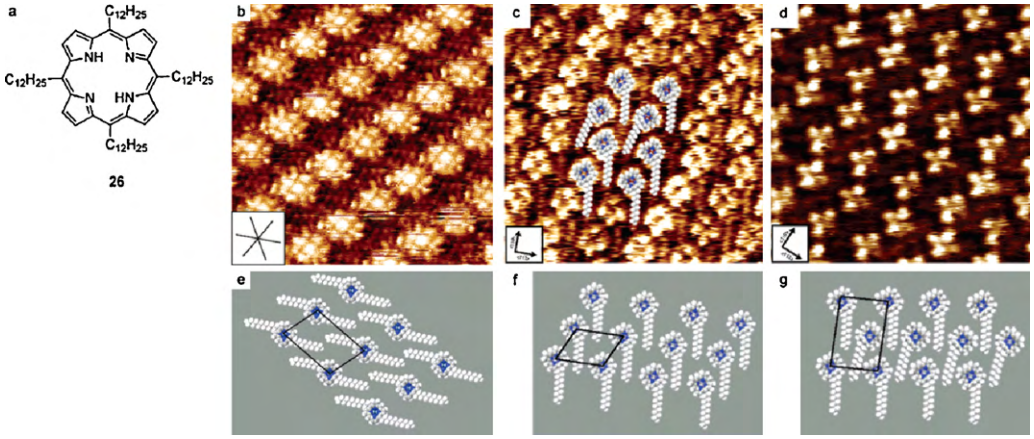

Fig. 11. (a) Molecular structure of the investigated porphyrin **26**. (b) STM image (8.1 nm × 8.1 nm) of the self-assembly of **26** on HOPG. The orientation of the main axes of HOPG are shown in the inset. (c and d) STM images (9.5 nm × 9.5 nm and 8.4 nm × 8.4 nm respectively) of the two self-assemblies formed by **26** deposited on Au(1 1 1). (e–g) The proposed packing models for the assemblies shown in the corresponding STM images.
This figure was reproduced from reference [94], with the permission of the copyright holders.

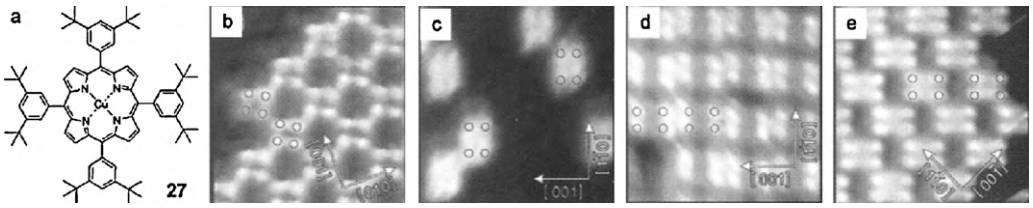

Fig. 12. (a) Molecular structure of the investigated porphyrin **27**. (b–e) STM images (10 nm × 10 nm) of **27** assembled on (b) Cu(1 0 0); (c) Au(1 1 0) in its kinetically favoured state; (d) Au(1 1 0) in its thermodynamically favoured state; (e) Ag(1 1 0).
This figure was reproduced from reference [95], with the permission of the copyright holders.

Cu(1 0 0), Au(1 1 0), and Ag(1 1 0) to determine what kind of conformational adaptations occur in the molecule in response to the substrate. The STM images obtained are shown in Fig. 12, displaying that a different assembly was obtained on each substrate. On the Cu surface, the di-*tert*-butylphenyl substituents maintained a 90° angle with respect to the porphyrin core. This conformation led to a square-shaped assembly (Fig. 12b). On the Au surface two distinct rotations of porphyrin **27** were observed corresponding to an anti-symmetric tilt of opposing substituents by 65° (Fig. 12c) and 45° (Fig. 12d). The latter rotational conformer is the thermodynamically stable form, which is predominant following long annealing cycles. It assembles as a close pack array on the surface. The most dramatic conformational change of **27** was observed on the Ag surface where the dihedral angle is 30° (Fig. 12e). These results clearly demonstrated the effect of the adsorbate–substrate interactions on assemblies. One year prior to this study, the same research group also showed that molecule **27** could be translocated on the Cu(1 0 0) surface using the STM tip [96]. These pioneering studies paved the way for more complex experiments under UHV conditions in the following years.

Expanding on the work of Yokoyama et al. that was described above [81], a series of studies involving a related set of cyanophenyl substituted porphyrins demonstrated that by taking advantage of the cyano groups' dipole–dipole and H-bonding intermolecular interactions 2D networks could be prepared on metal surfaces [52]. Also, the 2D networks formed could be used to host C_{60} molecules. The study of C_{60}-porphyrin interactions on surfaces was largely unexplored prior to these experiments [97]. The first study by Bonifazi et al. [52] investigates the self-assembly of a triply fused diporphyrin tape (**28**, Fig. 13a) and the monoporphyrin analogue (**29**, Fig. 13d) on Ag(1 0 0) surfaces under UHV conditions, and the subsequent hosting of C_{60} upon the formed 2D networks. At a coverage of 0.2–0.5 monolayer (ML) of **28** on a Ag(1 0 0) surface, ordered islands were observed with each diporphyrin unit being represented as a group of four bright lobes corresponding to the four 3,5-di-*tert*-butylphenyl substituents due to these groups preferential tunnelling transport. At approximately 1.0 ML coverage, molecule **28** organises into regular molecular rows (Fig. 13b) with a high packing density. 0.02 ML of C_{60} was sublimed onto this 2D network, which resulted mainly in the formation of unidirectional chains of various lengths, represented in the STM images as bright spherical protrusions (Fig. 13c). The C_{60} molecules assembled precisely on top of the cyanophenyl substituents at intermolecular distances of 2.2 nm. It was also confirmed that the fullerenes were non-covalently located above the porphyrin network, as a series of STM manipulations showed that individual C_{60} molecules could be relocated without disrupting the underlying monolayer. A similar experiment was also performed on a self-assembled monolayer of **29** (0.85 ML) on a Ag(1 0 0) surface (Fig. 13e). Sublimation of 0.14 monolayer of C_{60} onto a preformed array of **29** resulted in an unprecedented organisation of the fullerenes in vertically aligned pairs (Fig. 13f). In this case, the monolayer of **29** reorganizes upon deposition of C_{60} to better accommodate the incoming molecules. This assembly (C_{60}-**29**) has a higher thermal stability in compari-

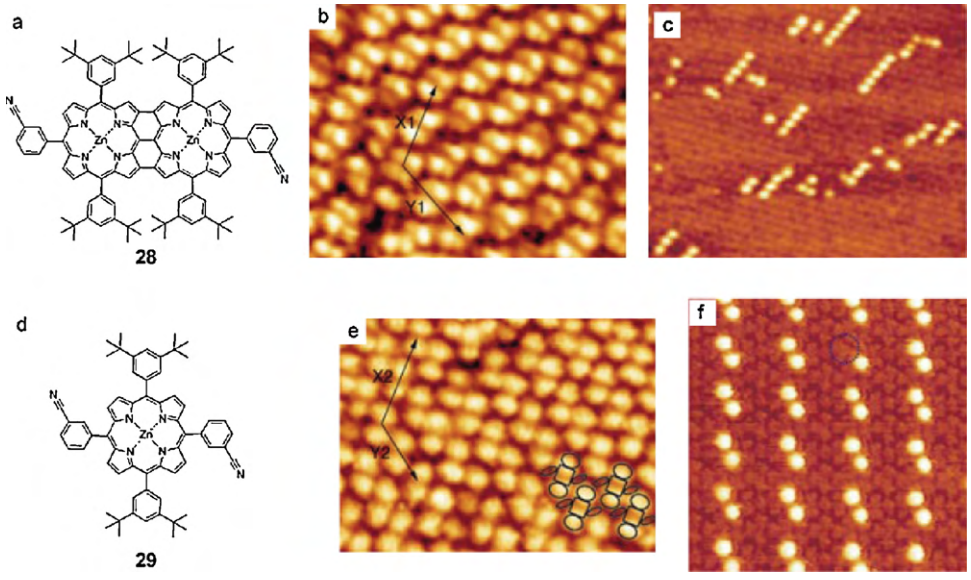

Fig. 13. (a and d) Molecular structures of investigated porphyrins **28** and **29**. (b) STM image (15.8 nm × 11.9 nm) of a monolayer of **28** sublimed on Ag(1 0 0). (c) STM image (77 nm × 65 nm) of C_{60} sublimed onto a monolayer of **28**. (e) STM image (12.2 nm × 9.1 nm) of a monolayer of **29** sublimed on Ag(1 0 0). (f) STM image (30 nm × 30 nm) of C_{60} sublimed onto a monolayer of **29**.
This figure was reproduced from reference [52], with the permission of the copyright holders.

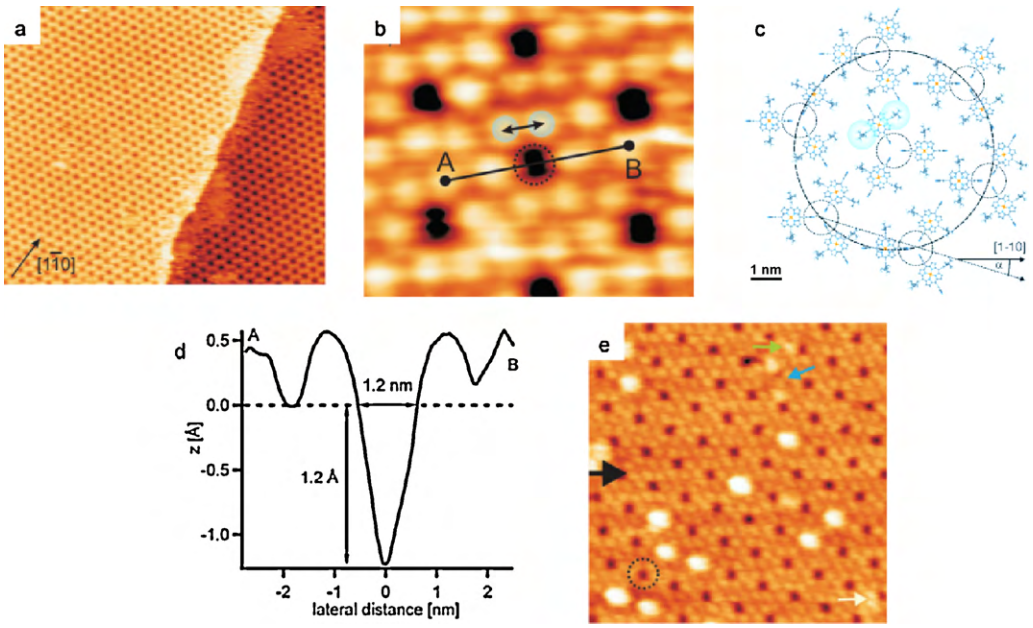

Fig. 14. (a) STM image (96 nm × 83 nm) of the porous network formed by the self-assembly of **29** on Ag(1 1 1). (b) Zoom-in of the STM image (9.1 nm × 8.0 nm). (c) The proposed model of the self-assembled porous network, the small circles indicate the pores. (d) The cross-section profile of a single pore scanned from A to B in (b). (e) STM image (30 nm × 30 nm) of the self-assembly following the sublimation of C_{60} molecules.
This figure was reproduced from reference [98], with the permission of the copyright holders.

son to the C_{60}-**28** assembly. At time, was clear evidence reported to unravel the self-assembly mechanism of this unprecedented hybrid C_{60}-**29** architecture.

Using the same porphyrin, **29**, Spillmann et al. [98] demonstrated that it was also possible to form porous networks under UHV conditions on a Ag(1 1 1) surface at a coverage of 0.5–0.7 ML (Fig. 14a). The primary driving forces for the formation of the porous networks were the previously described interactions between the cyanophenyl moieties (Fig. 4), that are dipole–dipole and van der Waals interactions. As shown in Fig. 14c, the formation of trimeric units with a central cavity (diameter ≈ 1.2 nm, Fig. 14d) fits well with the array observed by STM (Fig. 14b). In addition to the aforementioned intermolecular interactions, the Ag(1 1 1) substrate is thought to play a role in the formation of the hexagonal pores since the cyano functional groups can act as donating ligands coordinating to Ag ions, a well-known and strong interaction. Following the formation of the cavities in this self-assembly, 0.01 ML of C_{60} guests were introduced, which were mainly hosted at the pore sites (Fig. 14e). The fullerenes were mobile, hopping from pore to pore at a rate of 10^{-3} s^{-1} at room temperature. Gradually increasing the coverage of C_{60} led to formation of supramolecular islands of the guests, including linear hosted fullerene chains at 0.02 ML, branched chains and large islands at 0.07 ML, saturation of all the pores at 0.1 ML and finally the irreversible collapse of the 2D porous network of porphryin at monolayer coverages greater than 0.1 ML. These changes were also accompanied by a gradual reduction in the mobility of the guest molecules. Yokoyama and co-workers also reported the hosting of C_{60} molecules by arrays of porphyrin **30** (5,15-bis(4-carboxyphenyl)-10,20-bis(3,5-di-t-butyl-phenyl)porphyrin). Deposition of **30** on Au(1 1 1) under UHV results in the formation of a close packed network of molecular wires. Immediately after the adsorption of C_{60}, the wires shift laterally resulting in a nanoporous structure that is able to accommodate guest molecules [99].

Structural modification of **29** to include 4-cyanophenyl moieties (**31**, Fig. 15a), results in a molecule almost identical to **8**, differing only in the metal center, that is a zinc-porphyrin rather than a free base. The self-assembly of this species (**31**) was investigated by Diederich and co-workers on Cu(1 1 1) surfaces under UHV [100]. Upon vapour deposition, regular homochiral nanoporous domains formed (Fig. 15b). Each pore in the network displays a chiral windmill-shaped structure consisting of six wings, where the bright spot corresponding to each wing represents two *tert*-butyl residues of the 3,5-di(*tert*-butyl)phenyl substituents. Interestingly, these porous networks were able to host unbounded single porphyrin guests, which nested atop of each windmill-like cavity (Fig. 15c and d). At different temperatures the porphyrin guests could thermally switch from one stable position to another (shown by the horizontal lines in Fig. 15c and d). The guest molecules on the nanoporous network could also be manipulated individually by applying a local voltage by placing the STM tip above the chosen porphyrin guest under scanning conditions. Applying short pulses (∼1 s) resulted in single switching events, however, attempts to control the direction of rotation (*i.e.*, clockwise or counterclockwise) was not successful.

As an extension of the precedent studies, Wintjes et al. recently reported a systematic study on the influence of different alkoxyphenyl substituents on the porosity of porphyrin-based assemblies on Cu(1 1 1) under UHV conditions [101]. The self-organisation of three different porphyrin derivatives (**32**, **33** and **34**) was investigated (Fig. 16). Each porphyrin features two 4-cyanophenyl substituents in opposing *meso*-positions of the porphyrin core, however, the remaining *meso*-substituents differ bearing various types of alkoxyphenyl substituents. The variation of the alkoxyphenyl moieties controls the dimensionality of the resultant porous networks, altering the pore-to-pore distance in each assembly (3.09 ± 0.2 nm, 3.35 ± 0.12 nm and 4.80 ± 0.14 nm for assemblies of **32**, **33** and **34** respectively). Despite the changes in the pore-to-pore distances, the dimensions of individual pores remained unchanged in all the assemblies. At coverage below 0.8 ML, only porphyrin **32** self-assembles into a nanoporous hexagonal network (Fig. 16a), whereas porphyrins **33** and **34** form long chains with branching at random intervals. At higher coverage (>0.8 ML), as shown in Fig. 16b and c, porphyrins **32** and **33** also assemble into 2D porous networks. The assemblies of **32** and **33** (Fig. 16a and b) consisted of dimeric and trimeric supramolecular modules pro-

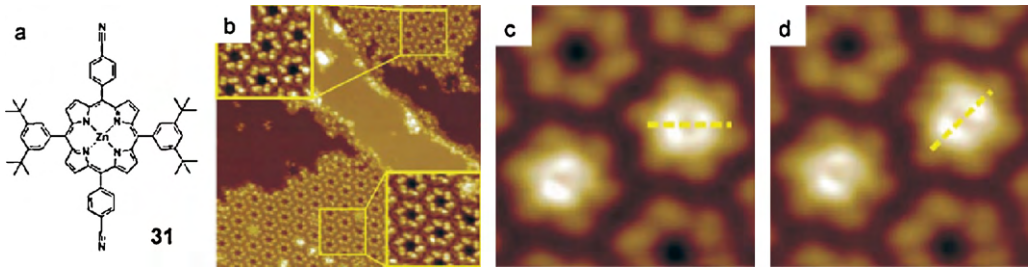

Fig. 15. (a) Molecular structure of the investigated porphyrin **31**. (b) STM image (50 nm × 50 nm) of the self-assembled network on Cu(1 1 1). The insets (9.1 nm × 9.1 nm) show that two homochiral domains were observed; (b and c) STM images (6.5 nm × 6.5 nm) showing the controlled rotation of the nested guest molecules induced by the STM tip.
This figure was reproduced from reference [100], with the permission of the copyright holders.

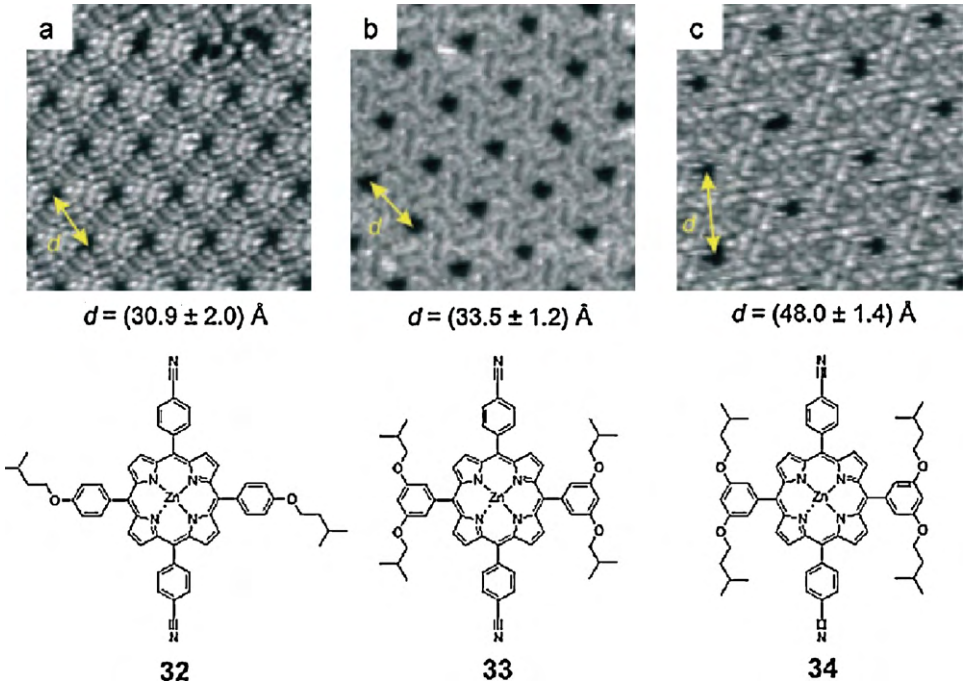

Fig. 16. (a–c) STM images (all 15 nm × 15 nm) of the nanoporous networks formed on Cu(1 1 1) by the porphyrins **32**–**34** shown below the respective images.
This figure was reproduced from reference [101], with the permission of the copyright holders.

duced via dipolar interactions of two or three cyanophenyl groups. However, porphyrin **34**, bearing the isopentyloxy substituents assembled through a different trimeric asymmetric non-covalent motif (Fig. 16c). One of two cyanophenyl groups of adjacent porphyrins forms a C≡N···H–C hydrogen-bond with the *ortho*-polarised C–H residue belonging to the phenyl ring bearing two electronegative alkoxy groups in a third neighbouring porphyrin.

4. Towards the 3rd dimension: from structures to functionality

Extension of porphyrin supramolecular assemblies on surfaces into the third dimension has been achieved in two ways. Friedlein et al. were able to achieve films with a thickness of several nanometres by the self-assembly of porphyrins into vertical columnar stacks that were perpendicular to the basal plane of the substrate [102]. A more common approach is to introduce a metal in the centre of a porphyrin's tetrapyrrolic macrocycle which can be exploited via axial coordination interactions to extend supramolecular assemblies on surfaces into the third dimension. Using the axial coordination approach, Otsuki et al. [103] synthesised three double-decker complexes of cerium(IV) with porphyrin or phthalocyanine ligands (**35**–**37**, Fig. 17a), and subsequently investigated their self-assembly at the 1-phenyloctane/HOPG interface by STM. All three complexes share a common porphyrin, 5,10,15,20-tetrakis(4-docosyloxyphenyl)porphyrin (C_{22}OPP), bearing long alkoxy chains to ensure the adsorption on HOPG of both heteroleptic complexes (**35** and **37**) and robust assemblies through close-packed arrays on HOPG. The other macrocycle in complex **35** was phthalocyanine (Pc), whereas in **37**, 5,15-bis-[4-(phenylethynyl)phenyl]porphyrin (BPEPP) was used. Ordered monolayers of each of the three complexes were observed upon deposition of their solutions onto HOPG. Complex **35** formed rows of bright circular spots corresponding to the Pc moieties, separated by dark rows corresponding to the interdigitated aliphatic chains adsorbed to the surface (Fig. 17b). Homoleptic complex **36** formed a similar stripped self-assembly with the bright protrusions having a square shape with the corners likely to correspond to the phenylene groups (Fig. 17c). Complex **37** also assembled in rows with the bright protrusions having an elliptical shape representing the BPEPP moiety (Fig. 17d). In a final experiment, a mixed solution of **37** and free-base porphyrin H_2(C_{22}OPP) was deposited on the HOPG surface, showing the presence of the double-decker complexes among the free-base porphyrins as bright protrusions (Fig. 17e). The height

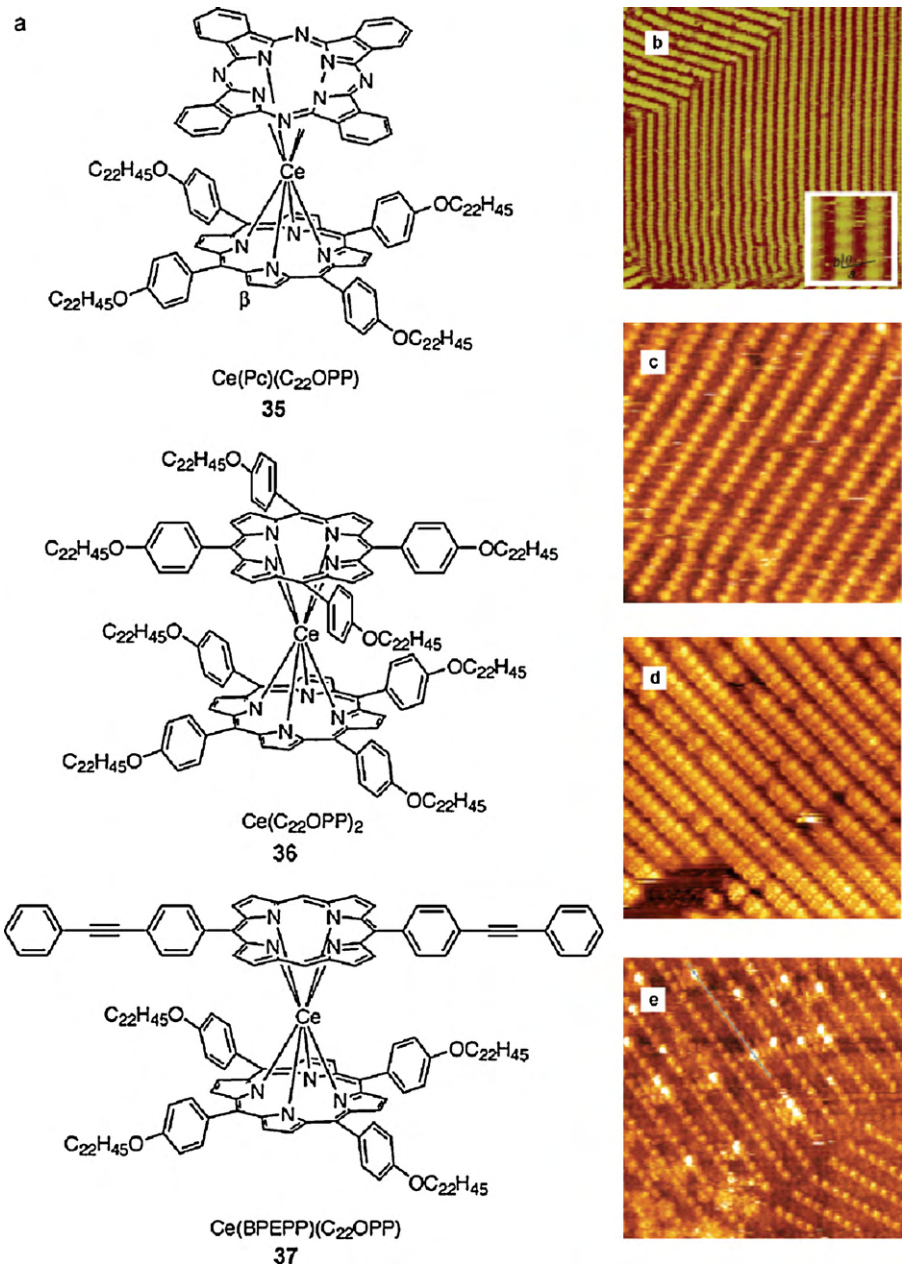

Fig. 17. (a) Molecular structures of the investigated double-decker porphyrins **35**, **36** and **37**. (b) STM images (100 nm × 100 nm) of **35**, (c) (50 nm × 50 nm) of **36**, (d) (50 nm × 50 nm) of **37**, (e) STM image (50 nm × 50 nm) of **37** mixed with two equivalents of $H_2(C_{22}OPP)$ at the 1-phenyloctane–HOPG interface.
This figure was reproduced from reference [102], with the permission of the copyright holders.

profile of the STM image indicated that the average height of the $H_2(C_{22}OPP)$ molecules was ~0.2 nm, whereas that of molecule **37** was 0.7–0.8 nm. Additionally, when complex **37** was flanked by free-base porphyrins, the shape was no longer elliptical, but isotropic, probably indicating a rotation of the upper macrocycle.

Shimizu and co-workers [104] also investigated the assembly of 3D coordinated porphyrins on HOPG surfaces. Four related porphyrins, bearing long alkoxy chains, were investigated (Fig. 18a). Two free-base porphyrins were synthesised, 5,10,15,20-tetrakis(4-octadecyloxyphenyl)porphyrin ($H_2(C_{18}OPP)$, **38**) and tetrakis(4-triacontyloxyphenyl)porphyrin ($H_2(C_{30}OPP)$, **39**), as well as their counterparts possessing a rhodium chloride metal centre coordinating a pyridine molecule, abbreviated as [Rh(C_{18}OPP)(Cl)(Py)] (**40**) and [Rh(C_{30}OPP)(Cl)(Py)] (**41**). Depositions of **38** and **39** onto HOPG (Fig. 18b and c) resulted in the highly ordered self-assembled rows of porphyrin cores (bright) separated by interdigitated alkoxy chains (dark). Only noisy STM images were obtained for the deposition of **40**, although glimpses of the self-assembled structure were observed (Fig. 18d). Deposition of **41** did not present such problems, presumably since the presence of longer alkyl chains results in a higher adsorption energy (Fig. 18e). A comparison of the average height profiles of the bright protrusions in the assemblies of porphyrins **39** (0.20 ± 0.03 nm) and **41** (0.43 ± 0.04 nm) confirmed that the pyridine molecule was indeed coordinated to the porphyrin central core in the assembly of **41**. Two mixed deposition experiments of **38** with **40**, and **39** with **41** resulted in the assemblies shown in Fig. 18f and g, displaying a nice contrast of dark spots and bright spots in both cases. Height profile examination confirmed that the dark spots corresponded to the free-base porphyrins in both cases, and the bright spots represented the pyridine coordinated porphyrins, further confirming the successful formation of a three-dimensional assembly.

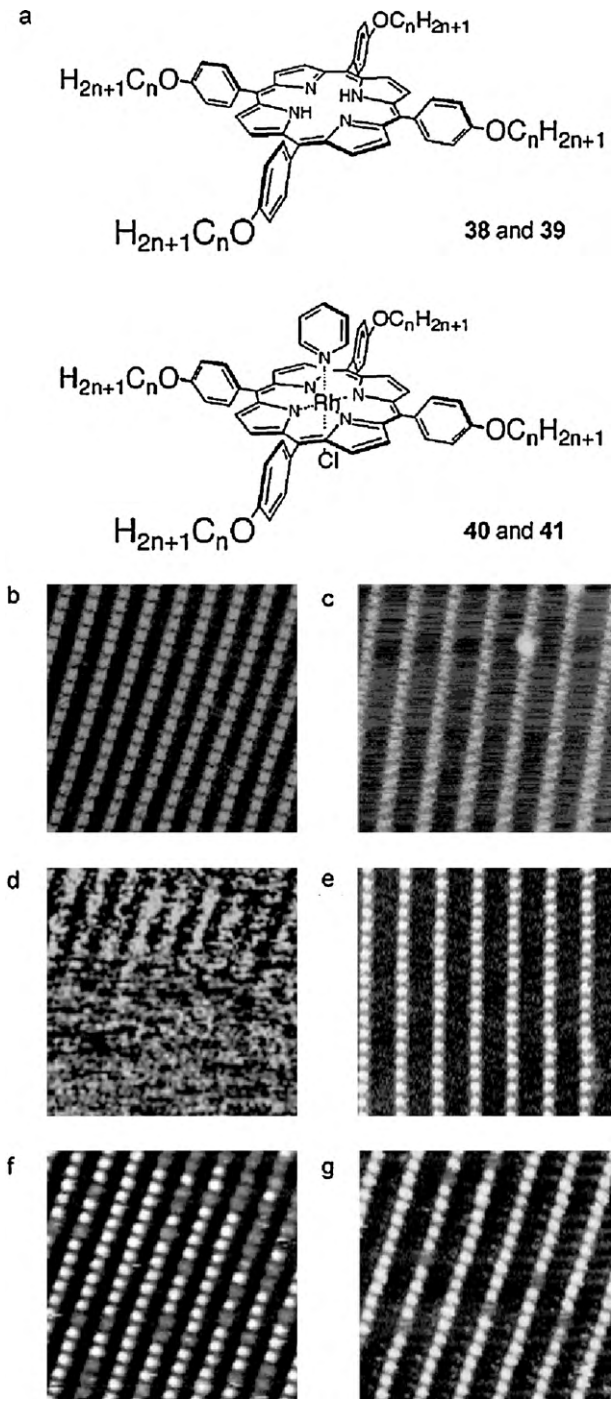

Fig. 18. (a) Molecular structures of the investigated porphyrins, **38** (n = 18), **39** (n = 30), **40** (n = 18) and **41** (n = 30). (b–g) STM images (35 nm × 35 nm) of the monolayers at the liquid–HOPG interface of: (b) **38**; (c) **39**; (d) **40**; (e) **41**; (f) 1:9 mixture of **38**/**40**; (g) 1:9 mixture of **39**/**41**. Solvents: 1-phenyloctane for **38** and **40**, and 1,2-dichlorobenzene for **39** and **40**.
This figure was reproduced from reference [103], with the permission of the copyright holders.

A recent paper by Feringa and co-workers [105] expands on the work of Shimizu and co-workers [104]. Zn(II)-metallated 5,10,15,20-tetradodecylporphyrin **42** porphyrin was deposited onto the HOPG in a *n*-tetradecane solution. An analogous self-assembly to that of **26** was obtained (Fig. 19a). The same experiment was repeated with 3-nitropyridine (**43**) coordinating to the zinc in **42** in solution prior to deposition, and once again an analogous assembly was obtained (Fig. 19b). The experiment was repeated with varying concentrations of **43** in a solution of **42** that was deposited onto HOPG (Fig. 19c shows an example of an STM image at 0.02:1 ratio of **43**:**42**). At every concentration examined, the percentage of coordinated porphyrins on the surface was higher than the percentage ratio of **43**:**42**. This indicated that it is likely that both an enhancement of **42**'s coordination affinity exists when it is physisorbed on HOPG compared to coordination in the bulk solution, and that the coordinated porphyrins physisorbed onto HOPG with greater affinity than uncoordinated porphyrins.

Similar experiments involving the construction of 3D systems under UHV conditions have also been performed. Lambert and co-workers, in 2004, reported that the zinc analogue of Cu-porphyrin (**27**) used by Jung et al. [95,96] *i.e.*, zinc tetra-(3,5-di-*tert*-butylphenyl)porphyrin (**44**) deposited onto Ag(1 0 0) could be reversibly capped by 1,4-diazabicylco[2.2.2]octane (DABCO, **45**) coordinating to **44** via one of the N atoms [106]. In subsequent work, the same group have reported the construction of chemically switchable molecular pinwheel using the same porphyrin with 4-methoxypyridine (**46**) as ligand [107]. Upon sublimation of pyridine ligand **46** onto a submonolayer coverage of **44** (at 123 K), the four-lobed porphyrin structures became 'doughnut'-shaped (height ≈ 4 Å, diameter ≈ 25 Å, Fig. 20b). Heating the assembly to 298K, the system returned to the original state, indicating the selective desorption of ligand **46**. The interesting feature of this assembly is that even though the apparent height of the assembly increased as expected, the height profile bore the same characteristic shape as a bare porphyrin molecule. Fig. 20c shows a comparison of the height profiles of bare **44**, **44** with coordinated DABCO and with 4-methoxypyridine. There is a clear difference between the profiles of the two coordinated porphyrins. Tetrapyrrolic module **44** in the presence of DABCO appeared as a circular bright protrusion (Fig. 20c) indicating that the DABCO coordinated to the upper face of **44**. In contrast, molecule **44** in the presence of **46** displayed a distinct central depression (Fig. 20c), therefore it is unlikely that the pyridyl ligand is coordinated to the upper face of the porphyrin macrocycle. Consequently, the authors concluded that ligand **46** is located beneath the porphyrin macrocycle acting as a tether, coordinating to the Ag surface with the O atom, and to the Zn-porphyrin with the aromatic N atom. This would enable the lifting of the porphyrin by ∼1 Å, weakening its interaction with the surface, consequently allowing the macrocycle to rotate, resulting in the time-averaged 'doughnut'-shaped protrusion observed in the STM image, resembling a molecular pinwheel device with ligand **46** acting as a pivotal axe (bottom right of Fig. 20c).

Further studies utilise coordinative interactions to metalloporphyrins in the third dimension to introduce other types of functionality such as catalysis. An example of such work takes us back to the early reports of Itaya and co-workers [91], where highly organised adlayers of Co(II) tetra-*meso*-phenylporphyrin (**47**) were prepared (see Section 3.1) on Au(1 1 1) electrode surfaces. In a study of the electrocatalytic activity for O_2 reduction to H_2O_2, Au electrodes with adsorbed monolayers of porphyrin **47** were able to enhance the reduction process in comparison to bare Au electrodes. Cyclic voltammograms (CVs) for the reduction process using both types of electrodes were obtained in 0.1 M $HClO_4$ solution saturated with O_2. The bare Au(1 1 1) electrode (top, Fig. 21) showed that the O_2-centered cathodic current started at approximately 0.55 V and gradually increased until −0.1 V. In contrast, the CV of the electrode bearing the monolayer of **47** (bottom, Fig. 21) showed that the O_2-centered cathodic current started at around 0.55 V during the scan and gave a clear electrocatalytic reduction peak for O_2 at 0.32 V, which after 0.3 V remained quite constant as the process was limited by the gas diffusion. The enhancement of current intensity

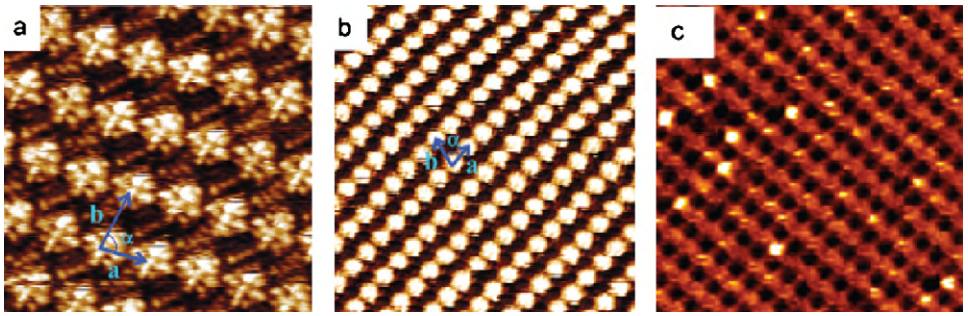

Fig. 19. (a) STM image (9.3 nm × 9.3 nm) at the *n*-tetradecane–HOPG interface of a self-assembled monolayer of **42**. (b) STM image (20.8 nm × 20.8 nm) at the *n*-tetradecane–HOPG interface of a self-assembled monolayer of **42** featuring **43** coordinated axially to the zinc metal centre. (c) STM image (20 nm × 20 nm) at the *n*-tetradecane–HOPG interface of a self-assembled monolayer of **42** following the addition of 2% of **43** to the *n*-tetradecane solution.
This figure was reproduced from reference [104], with the permission of the copyright holders.

at 0.32 V demonstrated that the self-assembled metalloporphyrin-based monolayer was catalysing the reduction of O_2 to H_2O_2.

In a more recent work published by Itaya and co-workers [108], adlayers of Co(II) 5,10,15,20-tetrakis(α,α,α,α-2-pivalamidophenyl)porphyrin (48, Fig. 22a) were prepared on Au electrodes. This porphyrin, nicknamed as 'picket-fence' porphyrin, is particularly interesting as its O_2 binding affinity is higher than that of native myoglobin [109,110]. Adlayers of 48 were thus prepared on both Au(1 1 1) and Au(1 0 0)-(hex) surfaces (for the method see Section 3.1). Nanobelt arrays were formed in both cases (an example is shown in Fig. 22b). However, when the deposition of O_2-adducted **48** molecules was attempted, nanobelt arrays were only formed on the Au(1 0 0)-(hex) surface. No ordered arrays were observed on Au(1 1 1), thus signifying that the adlayer formation is dependant on the crystallographic orientation of Au. It is suggested that underlying Au atoms can act as axial ligands assisting the formation of O_2-adducted **48** molecules. Nonetheless, on both surfaces, a mixture of bright and dark spots corresponding to porphyrin macrocycles was observed in the STM images (an example is shown in Fig. 22c). The bright spots are attributed to the O_2-adducted **48** molecules. Time-dependent STM images showed that the coordinated oxygen molecules were highly mobile, having the ability to move from one 'picket-fence' to another. Further investigation of the system showed that potential manipulations enabled the electrocatalytic reduction of the oxygen molecules in the cavities of **48** molecules. Moreover, small stepwise negative shifts in the potential (0.80 V, 0.78 V, 0.73 V and 0.68 V, Fig. 22d–f) led to the gradual reduction

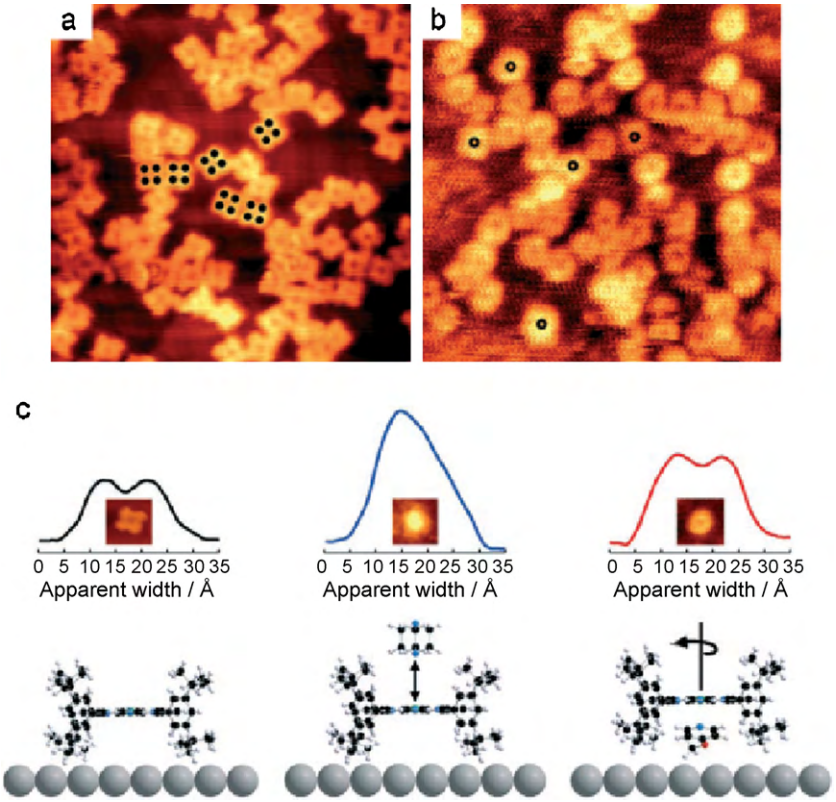

Fig. 20. (a and b) STM images (20 nm × 20 nm) showing a submonolayer coverage of **44** adsorbed on Ag(1 0 0): (a) before and (b) after the addition of 4-methoxypyridine on **46**. (c) Height profiles and structural scheme for: (left) bare **44** on Ag(1 0 0); (middle) the effect of capping **44** with DABCO, **45**; (right) the effect of inserting the 4-methoxypyridine "axle".
This figure was reproduced from reference [106], with the permission of the copyright holders.

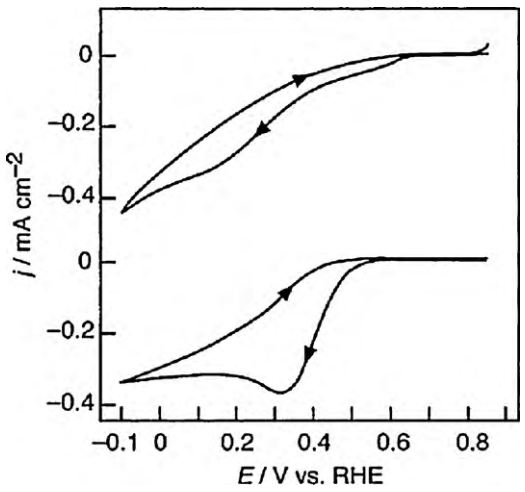

Fig. 21. Cyclic voltammograms for the O_2 reduction at the bare Au(1 1 1) electrode (top) and the electrode with **47** adsorbed (bottom). The CVs were performed in 0.1 M $HClO_4$ saturated with O_2 with potential scan rate of 50 mV s^{-1}.
This figure was reproduced from reference [91], with the permission of the copyright holders.

in coordinated oxygen molecules in the nanobelt array assembled on Au(1 0 0)-(hex), until at 0.65 V no more bright spots were observed in the STM images, thus indicating that all the O_2 had been released into solution. This final experiment indicates that the described system could function as a nanoscale oxygen storage device.

Oxidative catalytic activities have also been achieved using the axial coordination capacity of metalloporphyrins adsorbed as monolayers on surfaces. Hulsken et al. [111] were able to monitor the oxidation process of stilbene molecules in real time using STM at the liquid–solid interface. A Mn(III)-porphyrin was used in this study (**49**, Fig. 23a) as these metalloporphyrins catalyse the oxidation of alkenes to epoxides [35]. Self-assembly of **49** was initially investigated at the *n*-tetradecane/Au(1 1 1) interface under an Ar atmosphere. A regular patterned monolayer resulted, in which the porphyrin units adsorb face-on to the surface (Fig. 23b). The introduction of O_2 into the system led to the appearance of brighter spots, mainly in pairs, which corresponded to O_2-coordinated porphyrin **49** (Fig. 23c). This pairing is explicable as follows: O_2-Mn binding requires the metal's reduction, which in this case is thought to involve the Au substrate that coordinates to **49** axially allowing a chlorine radical to dissociate, reducing Mn(III) to Mn(II). Molecular O_2 then binds and reacts with the Mn(II) causing homolytic dissociation of O_2 to form two mono-oxygen-coordinated species, one of which coordinates to the closest adjacent **49** molecule. This results in a pair of reactive Mn(IV)═O species which can subsequently act as heterogeneous catalysts for the epoxidation reaction. The cycle is summarized in Fig. 23d. The epoxidation reaction using *cis*-stilbene was followed in real time and space by STM. Starting from a monolayer prepared under Ar, the number of oxidised **49** molecules in a fixed area of the surface were counted. O_2 molecules were then introduced to the system, causing an increase in the number of oxidised **49** molecules. Next, *cis*-stilbene was introduced, causing a significant drop in the number of oxidised **49** molecules. Gas chromatography analysis of the solution in the STM liquid-cell confirmed the presence of both *cis*-stilbene oxide and *trans*-stilbene oxide signifying that the surface catalytic device was functional. The monolayer was monitored for several days during which the number of oxidised **49** molecules remained constant following the reaction, demonstrating that the surface-bound catalysts were stable and also possess the potential for long-lasting activity.

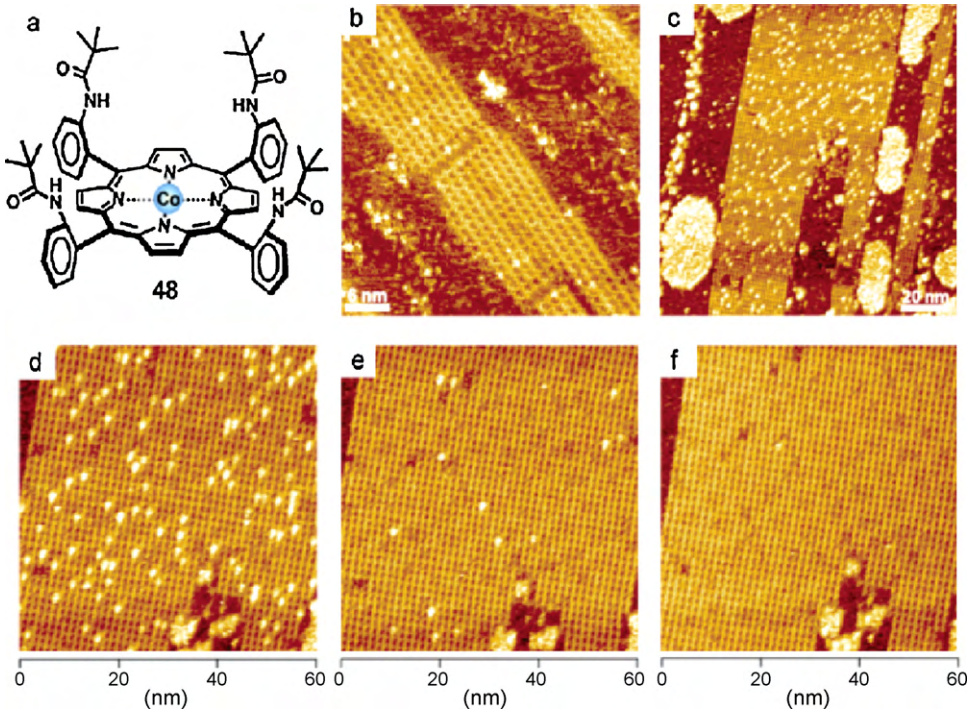

Fig. 22. (a) Structure of 'picket-fence' porphyrin **48**. STM images of the nanobelt arrays formed (b) (40 nm × 40 nm) by **48** on Au(1 1 1), (c) (125 nm × 125 nm) by **48** on Au(1 0 0)-(hex) at 0.8 V vs RHE in 0.1 M $HClO_4$, after immersion in an O_2 saturated solution. The bright spots indicate porphyrins with axially complexed O_2 molecules. (d–f) Potential dependent STM images (60 nm × 60 nm) of the array shown in (c) at (d) 0.78 V; (e) 0.73 V and (f) 0.68 V vs RHE in 0.1 M $HClO_4$, showing a gradual reduction in coordinated O_2 molecules.
This figure was reproduced from reference [107], with the permission of the copyright holders.

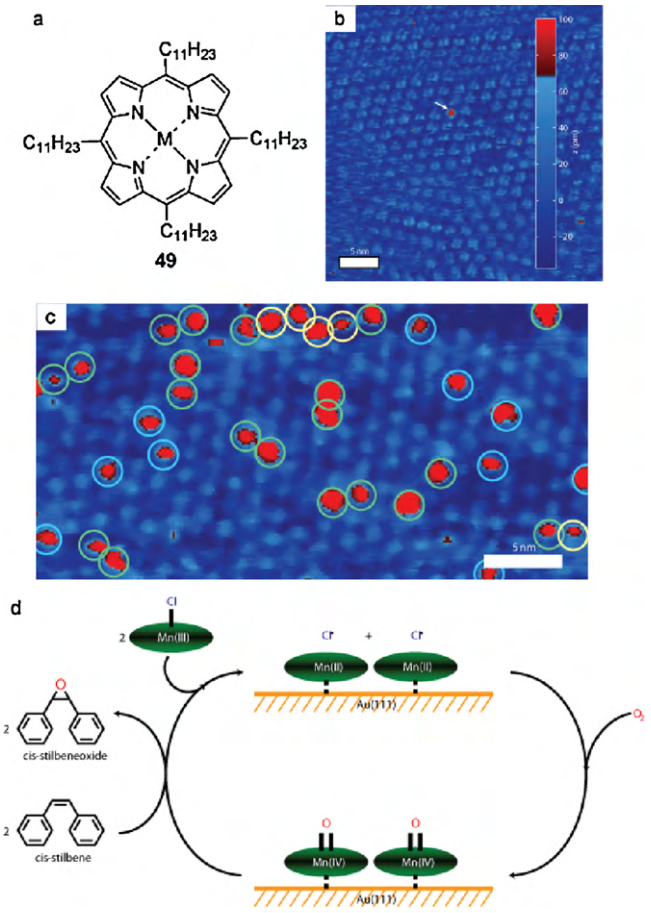

Fig. 23. (a) Molecular structure of porphyrin **49**, M = MnCl. (b) STM image of a monolayer of **49** self-assembled at an interface of Au(1 1 1) and an argon-saturated *n*-tetradecane liquid phase. (c) STM image of a monolayer of **49** self-assembled 4 h after the introduction of O_2. The overall population of bright spots corresponding to **49** with complexed O_2 is approximately 8%. (d) Proposed catalytic cycle of the epoxidation reaction.
This figure was reproduced from reference [110], with the permission of the copyright holders.

5. Concluding remarks

One of the main research areas at the boundary between chemistry and physics is the engineering of multifunctional organic materials, with exploitable properties for applications in materials science. Porphyrins represent one class of organic materials that is rigorously investigated in this respect since it is desirable to replicate the functions that these molecules perform in nature, *i.e.*, electron transfer, oxygen transfer, and light-harvesting. The macroscopic properties of such porphyrin-based materials can easily be controlled and manipulated via chemical functionalisation of the fundamental tetrapyrrolic macrocycle with a wide variety of organic groups, thus offering an exceptional molecular module for both revolutionising the optical and electronic components and also, for engineering superior functional molecular-based devices. The main challenge in the construction of such new devices is the strict control, location and accessibility of the molecular constituents. The active and greatly diversified research projects described above all contribute to conquering this challenge, which was particularly made possible with the advent of SPM techniques and in particular of STM. In this review, through the discussion of carefully chosen examples from the literature, we have illustrated the trends in supramolecular nanopatterning of porphyrin derivatives on surfaces. Solution-based supramolecular assemblies of porphyrin derivatives, as well as their applications, were initially discussed, however a new tendency in current research is to deposit functional porphyrin derivatives on the surfaces of bulk materials such as metals or semiconductors and investigate the resultant hybrid surfaces using STM techniques. Various strategies for the construction of nanoscale architectures on surfaces are described along the course of the review, including sublimation under UHV conditions, adlayer formation by immersion of surfaces into solutions and also the deposition of solutions directly onto the surface for the direct investigation at the liquid–solid interface. The discussion of assemblies on surfaces commences with very recent developments in the remarkably precisely controlled construction of discrete assemblies on surfaces under UHV conditions. The formation of 1D molecular chains is also briefly mentioned in this section. Subsequently, extended 2D arrays formed in both ambient conditions at the liquid–solid interface, as well as under UHV conditions are discussed. The ability of certain 2D self-assemblies to host guest molecules is also illustrated. Finally, a section devoted to the building of porphyrin assemblies displaying three-dimensional features followed, detailing the description of the coordination capacity of certain metalloporphyrins to engineer functional materials with potential applications in molecular rotors, catalytic devices and gas storage systems. However, this review represents recent advances in the literature that can still be considered as the initial stages towards the design and production of functional supramolecular arrays [112], which could eventually be included in devices that are functional at the macroscopic level. Even though no solar cells, fuel cells, data storage devices nor any other final application can be reported yet, the discussed prototypic examples illustrate how carrying out innovative and creative research using the "bottom-up" approach is getting closer to the ultimate goal of producing real-world technologies.

Acknowledgements

This work was supported by the European Union through the Marie-Curie Research Training Network "PRAIRIES", contract MRTN-CT-2006-035810, the Marie-Curie Initial Training Network "FINELUMEN", grant agreement PITN-GA-2008-215399, INSTM, the Belgian National Research Foundation (FRS-FNRS) (through the contracts no. 2.4.625.08 and 2.4.550.09), "Loterie Nationale", the 'TINTIN' ARC project from the Belgian French Community, the FSR grant, the Région Wallonne, the University of Trieste and the University of Namur. SM thanks the EU Marie-Curie Research Training Network "PRAIRIES" and the University of Namur for his doctoral fellowship. Dr. H. Spillmann and Dr. M. Sthör (University of Basel, CH), Dr. T. Jung (Paul Scherrer Institut, CH), Prof. J.V. Barth, Dr. W. Auwärter (Technical University of Munich, DE) and Prof. P. Samori (ISIS-University of Strasbourg, FR) are especially acknowledged for their fruitful collaboration and contribution throughout these years for our achievements on supramolecular porphyrin-based netstudies studied by STM.

References

[1] Y. Yang, F. Wudl, Adv. Mater. 21 (2009) 1401.
[2] M. Busi, M. Laurenti, G.G. Condorelli, A. Motta, M. Favazza, I.L. Fragalà, M. Montalti, L. Prodi, E. Dalcanale, Chem. Eur. J. 13 (2007) 6891.
[3] E. Menozzi, R. Pinalli, E.A. Speets, B.J. Ravoo, E. Dalcanale, D.N. Reinhoudt, Chem. Eur. J. 10 (2004) 2199.
[4] E. Biavardi, M. Favazza, A. Motta, I.L. Fragalà, C. Massera, L. Prodi, M. Montalti, M. Melegari, G.G. Condorelli, E. Dalcanale, J. Am. Chem. Soc. 131 (2009) 7447.
[5] L.J. Prins, D.N. Reinhoudt, P. Timmerman, Angew. Chem. Int. Ed. 40 (2001) 2382.
[6] Special issue on "Supramolecular Chemistry and Self-Assembly", in: Science, 2002, p. 2396.
[7] A. Mammana, A. D'Urso, R. Lauceri, R. Purrello, J. Am. Chem. Soc. 129 (2007) 8062.

[8] F.J.M. Hoeben, P. Jonkheijm, E.W. Meijer, A. Schenning, Chem. Rev. 105 (2005) 1491.
[9] D.M. Guldi, F. Zerbetto, V. Georgakilas, M. Prato, Acc. Chem. Res. 38 (2005) 871.
[10] K. Yoosaf, A. Belbakra, N. Armaroli, A. Llanes-Pallas, D. Bonifazi, Chem. Commun. (2009) 2830.
[11] G.G. Condorelli, A. Motta, M. Favazza, E. Gurrieri, P. Betti, E. Dalcanale, Chem. Commun. 46 (2010) 288.
[12] L. Pirondini, A.G. Stendardo, S. Geremia, M. Campagnolo, P. Samorì, J.P. Rabe, R. Fokkens, E. Dalcanale, Angew. Chem. Int. Ed. 42 (2003) 1384.
[13] M. Tonezzer, M. Melegari, G. Maggioni, R. Milan, G.D. Mea, E. Dalcanale, Chem. Mater. 20 (2008) 6535.
[14] T. Arai, K. Kobata, H. Mihara, T. Fujimoto, N. Nishino, Bull. Chem. Soc. Jpn. 68 (1995) 1989.
[15] T. Arai, K. Takei, N. Nishino, T. Fujimoto, Chem. Commun. (1996) 2133.
[16] H.A. Dailey, Biosynthesis of Heme and Chlorophylls, McGraw-Hill, New York, 1990.
[17] G.R. Geier, T. Sasaki, Tetrahedron Lett. 38 (1997) 3821.
[18] F. Rabanal, B.R. Gibney, W.F. DeGrado, C.C. Moser, P.L. Dutton, Inorg. Chim. Acta 243 (1996) 213.
[19] H. Imahori, T. Umeyama, J. Phys. Chem. C 113 (2009) 9029.
[20] S. Saha, E. Johansson, A.H. Flood, H.R. Tseng, J.I. Zink, J.F. Stoddart, Chem. Eur. J. 11 (2005) 6846.
[21] D.M. Guldi, H. Taieb, G.M.A. Rahman, N. Tagmatarchis, M. Prato, Adv. Mater. 17 (2005) 871.
[22] R.F. Kelley, W.S. Shin, B. Rybtchinski, L.E. Sinks, M.R. Wasielewski, J. Am. Chem. Soc. 129 (2007) 3173.
[23] M. Crute, Acta Crystallogr. 12 (1959) 24.
[24] E. Iengo, E. Zangrando, E. Alessio, Acc. Chem. Res. 39 (2006) 841.
[25] J.T. Falk, in: K.M. Smith (Ed.), Porphyrins and Metalloporphyrins, Elsevier, Amsterdam, 1975, p. 3.
[26] J.T. Falk, in: K.M. Smith (Ed.), Porphyrins and Metalloporphyrins, Elsevier, Amsterdam, 1975, p. 29.
[27] T.K. Ahn, K.S. Kim, D.Y. Kim, S.B. Noh, N. Aratani, C. Ikeda, A. Osuka, D. Kim, J. Am. Chem. Soc. 128 (2006) 1700.
[28] F.J.M. Hoeben, M. Wolffs, J. Zhang, S. De Feyter, P. Leclère, A.P.H.J. Schenning, E.W. Meijer, J. Am. Chem. Soc. 129 (2007) 9819.
[29] K. Kurotobi, K.S. Kim, S.B. Noh, D. Kim, A. Osuka, Angew. Chem. Int. Ed. 45 (2006) 3944.
[30] D. Kim, A. Osuka, Acc. Chem. Res. 37 (2004) 735.
[31] I.W. Hwang, T. Kamada, T.K. Ahn, D.M. Ko, T. Nakamura, A. Tsuda, A. Osuka, D. Kim, J. Am. Chem. Soc. 126 (2004) 16187.
[32] J. Aimi, K. Oya, A. Tsuda, T. Aida, Angew. Chem. Int. Ed. 46 (2007) 2031.
[33] A. Tsuda, S. Sakamoto, K. Yamaguchi, T. Aida, J. Am. Chem. Soc. 125 (2003) 15722.
[34] D. Bonifazi, G. Accorsi, N. Armaroli, F.Y. Song, A. Palkar, L. Echegoyen, M. Scholl, P. Seiler, B. Jaun, F. Diederich, Helv. Chim. Acta 88 (2005) 1839.
[35] B. Meunier, Chem. Rev. 92 (1992) 1411.
[36] P. Even, B. Boitrel, Coord. Chem. Rev. 250 (2006) 519.
[37] F. Diederich, B. Felber, Proc. Natl. Acad. Sci. U.S.A. 99 (2002) 4778.
[38] P. Facci, M.P. Fontana, E. Dalcanale, M. Costa, T. Sacchelli, Langmuir 16 (2000) 7726.
[39] C.D. Natale, R. Paolesse, A. Macagnano, S. Nardis, E. Martinelli, E. Dalcanale, M. Costa, A. D'Amico, J. Mater. Chem. 14 (2004) 1281.
[40] S. Yoshimoto, K. Itaya, J. Porphyr. Phthalocya. 11 (2007) 313.
[41] Y. Nakamura, N. Aratani, A. Osuka, Chem. Soc. Rev. 36 (2007) 831.
[42] J.S. Hu, Y.G. Guo, H.P. Liang, L.J. Wan, L. Jiang, J. Am. Chem. Soc. 127 (2005) 17090.
[43] A. Tsuda, H.F. Hu, R. Tanaka, T. Aida, Angew. Chem. Int. Ed. 44 (2005) 4884.
[44] K. Ogawa, T.Q. Zhang, K. Yoshihara, Y. Kobuke, J. Am. Chem. Soc. 124 (2002) 22.
[45] F. Hajjaj, Z.S. Yoon, M.C. Yoon, J. Park, A. Satake, D.H. Kim, Y. Kobuke, J. Am. Chem. Soc. 128 (2006) 4612.
[46] I. Goldberg, Chem. Commun. (2005) 1243.
[47] Z. Liu, A.A. Yasseri, J.S. Lindsey, D.F. Bocian, Science 302 (2003) 1543.
[48] P. Samorì, J. Mater. Chem. 14 (2004) 1353.
[49] P. Samorì, Chem. Soc. Rev. 34 (2005) 511.
[50] S. De Feyter, A. Gesquiere, M.M. Abdel-Mottaleb, P.C.M. Grim, F.C. De Schryver, C. Meiners, M. Sieffert, S. Valiyaveettil, K. Müllen, Acc. Chem. Res. 33 (2000) 520.
[51] S. De Feyter, F.C. De Schryver, Chem. Soc. Rev. 32 (2003) 393.
[52] D. Bonifazi, H. Spillmann, A. Kiebele, M. de Wild, P. Seiler, F.Y. Cheng, H.J. Güntherodt, T. Jung, F. Diederich, Angew. Chem. Int. Ed. 43 (2004) 4759.
[53] J.V. Barth, G. Costantini, K. Kern, Nature 437 (2005) 671.
[54] S. De Feyter, H. Uji-I, W. Mamdouh, A. Miura, J. Zhang, P. Jonkheijm, A.P.H.J. Schenning, E.W. Meijer, Z. Chen, F. Würthner, N. Schuurmans, J. Van Esch, B.L. Feringa, A.E. Dulcey, V. Percec, F.C. De Schryver, Int. J. Nanotechnol. 3 (2006) 462.
[55] L.J. Wan, Acc. Chem. Res. 39 (2006) 334.
[56] J.V. Barth, Annu. Rev. Phys. Chem. 58 (2007) 375.
[57] N. Miyashita, D.G. Kurth, J. Mater. Chem. 18 (2008) 2636.
[58] E. Gomar-Nadal, J. Puigmartí-Luis, D.B. Amabilino, Chem. Soc. Rev. 37 (2008) 490.
[59] A. Kühnle, Curr. Opin. Colloid Interface Sci. 14 (2009) 157.
[60] X. Ma, Y. Yang, K. Deng, Q. Zeng, K. Zhao, C. Wang, C. Bai, J. Mater. Chem. (2008) 2074.
[61] F. Cicoira, C. Santato, F. Rosei, Top. Curr. Chem. 285 (2008) 203.
[62] D. Bonifazi, O. Enger, F. Diederich, Chem. Soc. Rev. 36 (2007) 390.
[63] A. Llanes-Pallas, M. Matena, T. Jung, M. Prato, M. Stöhr, D. Bonifazi, Angew. Chem. Int. Ed. 47 (2008) 7726.
[64] T. Kudernac, S. Lei, J.A.A.W. Elemans, S. De Feyter, Chem. Soc. Rev. 38 (2009) 402.
[65] A.P. Alivisatos, P.F. Barbara, A.W. Castleman, J. Chang, D.A. Dixon, M.L. Klein, G.L. McLendon, J.S. Miller, M.A. Ratner, P.J. Rossky, S.I. Stupp, M.E. Thompson, Adv. Mater. 10 (1998) 1297.
[66] C.B. Gorman, R.L. Carroll, Angew. Chem. Int. Ed. 41 (2002) 4378.
[67] C. Joachim, M.A. Ratner, Proc. Natl. Acad. Sci. U.S.A. 102 (2005) 8801.
[68] J.S. Wu, W. Pisula, K. Müllen, Chem. Rev. 107 (2007) 718.
[69] A. Schenning, E.W. Meijer, Chem. Commun. (2005) 3245.
[70] H.C. Yang, T.J. Shin, L. Yang, K. Cho, C.Y. Ryu, Z.N. Bao, Adv. Funct. Mater. 15 (2005) 671.
[71] Special issue on "Supramolecular Approaches to Organic Electronics and Nanotechnology", in: Adv. Mater., 2006, p. 1227.
[72] J.E. Green, J.W. Choi, A. Boukai, Y. Bunimovich, E. Johnston-Halperin, E. DeIonno, Y. Luo, B.A. Sheriff, K. Xu, Y.S. Shin, H.R. Tseng, J.F. Stoddart, J.R. Heath, Nature 445 (2007) 414.
[73] A.R. Murphy, J.M.J. Fréchet, Chem. Rev. 107 (2007) 1066.
[74] H. Haick, D. Cahen, Acc. Chem. Res. 41 (2008) 359.
[75] R.H. Friend, R.W. Gymer, A.B. Holmes, J.H. Burroughes, R.N. Marks, C. Taliani, D.D.C. Bradley, D.A. Dos Santos, J.L. Brédas, M. Logdlund, W.R. Salaneck, Nature 397 (1999) 121.
[76] F. Cacialli, J.S. Wilson, J.J. Michels, C. Daniel, C. Silva, R.H. Friend, N. Severin, P. Samorì, J.P. Rabe, M.J. O'Connell, P.N. Taylor, H.L. Anderson, Nat. Mater. 1 (2002) 160.
[77] S.R. Forrest, Nature 428 (2004) 911.
[78] Y. Yamamoto, T. Fukushima, Y. Suna, N. Ishii, A. Saeki, S. Seki, S. Tagawa, M. Taniguchi, T. Kawai, T. Aida, Science 314 (2006) 1761.
[79] D.L. Taylor, E.S. Woo, K.A. Giuliano, Curr. Opin. Biotechnol. 12 (2001) 75.
[80] M. Sarikaya, C. Tamerler, A.K.Y. Jen, K. Schulten, F. Baneyx, Nat. Mater. 2 (2003) 577.
[81] T. Yokoyama, S. Yokoyama, T. Kamikado, Y. Okuno, S. Mashiko, Nature 413 (2001) 619.
[82] L.A. Fendt, M. Stöhr, N. Wintjes, M. Enache, T.A. Jung, F. Diederich, Chem. Eur. J. 15 (2009) 11139.
[83] J.V. Barth, H. Brune, G. Ertl, R.J. Behm, Phys. Rev. B 42 (1990) 9307.
[84] S. Maier, L.A. Fendt, L. Zimmerli, T. Glatzel, O. Pfeiffer, F. Diederich, E. Meyer, Small 4 (2008) 1115.
[85] D. Heim, K. Seufert, W. Auwarter, C. Aurisicchio, C. Fabbro, D. Bonifazi, J.V. Barth, Nano Lett. 10 (2009) 122.
[86] W. Auwärter, F. Klappenberger, A. Weber-Bargioni, A. Schiffrin, T. Strunskus, C. Wöll, Y. Pennec, A. Riemann, J.V. Barth, J. Am. Chem. Soc. 129 (2007) 11279.
[87] O. Shoji, H. Tanaka, T. Kawai, Y. Kobuke, J. Am. Chem. Soc. 127 (2005) 8598.
[88] O. Shoji, S. Okada, A. Satake, Y. Kobuke, J. Am. Chem. Soc. 127 (2005) 2201.
[89] S.H. Joo, S.J. Choi, I. Oh, J. Kwak, Z. Liu, O. Terasaki, R. Ryoo, Nature 412 (2001) 169.
[90] L. Grill, M. Dyer, L. Lafferentz, M. Persson, M.V. Peters, S. Hecht, Nat. Nanotechnol. 2 (2007) 687.
[91] S. Yoshimoto, A. Tada, K. Suto, R. Narita, K. Itaya, Langmuir 19 (2003) 672.
[92] S. Yoshimoto, N. Higa, K. Itaya, J. Am. Chem. Soc. 126 (2004) 8540.
[93] S. Yoshimoto, Y. Honda, O. Ito, K. Itaya, J. Am. Chem. Soc. 130 (2008) 1085.
[94] N. Katsonis, J. Vicario, T. Kudernac, J. Visser, M.M. Pollard, B.L. Feringa, J. Am. Chem. Soc. 128 (2006) 15537.
[95] T.A. Jung, R.R. Schlittler, J.K. Gimzewski, Nature 386 (1997) 696.
[96] T.A. Jung, R.R. Schlittler, J.K. Gimzewski, H. Tang, C. Joachim, Science 271 (1996) 181.
[97] J.K. Gimzewski, T.A. Jung, M.T. Cuberes, R.R. Schlittler, Surf. Sci. 386 (1997) 101.
[98] H. Spillmann, A. Kiebele, M. Stöhr, T.A. Jung, D. Bonifazi, F. Cheng, F. Diederich, Adv. Mater. 18 (2006) 275.
[99] F. Nishiyama, T. Yokoyama, T. Kamikado, S. Yokoyama, S. Mashiko, K. Sakaguchi, K. Kikuchi, Adv. Mater. 19 (2007) 117.
[100] N. Wintjes, D. Bonifazi, F.Y. Cheng, A. Kiebele, M. Stöhr, T. Jung, H. Spillmann, F. Diederich, Angew. Chem. Int. Ed. 46 (2007) 4089.
[101] N. Wintjes, J. Hornung, J. Lobo-Checa, T. Voigt, T. Samuely, C. Thilgen, M. Stöhr, F. Diederich, T.A. Jung, Chem. Eur. J. 14 (2008) 5794.
[102] R. Friedlein, X. Crispin, W. Osikowicz, S. Braun, M.P. de Jong, C.D. Simpson, M.D. Watson, F. von Kieseritzky, P. Samorí, S.K.M. Jönsson, M. Fahlman, F. Jäckel, J.P. Rabe, J. Hellberg, K. Müllen, W.R. Salaneck, Synth. Met. 147 (2004) 79.
[103] J. Otsuki, S. Kawaguchi, T. Yamakawa, M. Asakawa, K. Miyake, Langmuir 22 (2006) 5708.
[104] T. Ikeda, M. Asakawa, M. Goto, K. Miyake, T. Ishida, T. Shimizu, Langmuir 20 (2004) 5454.
[105] J. Visser, N. Katsonis, J. Vicario, B.L. Feringa, Langmuir 25 (2009) 5980.
[106] F.J. Williams, O.P.H. Vaughan, K.J. Knox, N. Bampos, R.M. Lambert, Chem. Commun. (2004) 1688.

[107] O.P.H. Vaughan, F.J. Williams, N. Bampos, R.M. Lambert, Angew. Chem. Int. Ed. 45 (2006) 3779.
[108] S. Yoshimoto, K. Sato, S. Sugawara, Y. Chen, O. Ito, T. Sawaguchi, O. Niwa, K. Itaya, Langmuir 23 (2006) 809.
[109] J.P. Collman, R.R. Gagne, T.R. Halbert, J.C. Marchon, C.A. Reed, J. Am. Chem. Soc. 95 (1973) 7868.
[110] J.P. Collman, R.R. Gagne, C. Reed, T.R. Halbert, G. Lang, W.T. Robinson, J. Am. Chem. Soc. 97 (1975) 1427.
[111] B. Hulsken, R. Van Hameren, J.W. Gerritsen, T. Khoury, P. Thordarson, M.J. Crossley, A.E. Rowan, R.J.M. Nolte, J.A.A.W. Elemans, S. Speller, Nat. Nanotechnol. 2 (2007) 285.
[112] D. Bonifazi, S. Mohnani, A. Llanes-Pallas, Chem. Eur. J. 15 (2009) 7004.